Supplementary Data

Supplementary data associated with this article can be found, in the online version, at doi;10.1053/j.gastro.2006.10.035.

References

1. Zeng D, Hoffmann P, Lan F, Huie P, Higgins J, Strober S. Unique patterns of surface receptors, cytokine secretion, and immune functions distinguish T cells in the bone marrow from those in the periphery: impact on allogeneic bone marrow transplantation. Blood 2002;99:1449–1457.
2. Di Rosa F, Pabst R. The bone marrow: a nest for migratory memory T cells. Trends Immunol 2005;26:360–366.
3. Mazo IB, Honczarenko M, Leung H, Cavanagh LL, Bonasio R, Weninger W, Engelke K, Xia L, McEver RP, Koni PA, Siberstein LE, von Andrian UH. Bone marrow is a major reservoir and site of recruitment for central memory CD8+ T cells. Immunity 2005;22:259–270.
4. Price PW, Cerny J. Characterization of CD4+ T cells in mouse bone marrow. I. Increased activated/memory phenotype and altered TCR Vβ repertoire. Eur J Immunol 1999;29:1051–1056.
5. Di Rosa F, Santoni A. Bone marrow CD8 T cells are in a different activation state than those in lymphoid periphery. Eur J Immunol 2002;32:1873–1880.
6. Benner R, Meima F, van der Meulen GM, van Muiswinkel WB. Antibody formation in mouse bone marrow. II. Evidence for a memory-dependent phenomenon. Immunology 1974;26:247–255.
7. Masopust D, Vezys V, Marzo AL, Lefrancois L. Preferential localization of effector memory cells in nonlymphoid tissue. Science 2001;291:2413–2417.
8. Reinhardt RL, Khoruts A, Merica R, Zell T, Jenkins MK. Visualizing the generation of memory CD4 T cells in the whole body. Nature 2001;410:101–105.
9. Slifka MK, Whitmire JK, Ahmed R. Bone marrow contains virus-specific cytotoxic T lymphocytes. Blood 1997;90:2103–2108.
10. Wherry EJ, Teichgraber V, Becker TC, Masopust D, Kaech SM, Antia R, von Andrian UH, Ahmed R. Lineage relationship and protective immunity of memory CD8 T cell subsets. Nat Immunol 2003;4:225–234.
11. Feuerer M, Beckhove P, Garbi N, Mahnke Y, Limmer A, Hommel M, Hammerling GJ, Kyewski B, Hamann A, Umansky V, Schirrmacher V. Bone marrow as a priming site for T-cell responses to blood-borne antigen. Nat Med 2003;9:1151–1157.
12. Munkholm P, Binder V. Clinical features and natural history of Crohn's disease. In: Kirsner JB, Shorter RB, eds. Inflammatory bowel disease. Baltimore: Williams & Wilkins, 2004:289–300.
13. Kameyama J, Sasaki I, Imamura M, Naito H, Sato T. Surgical treatment for Crohn's disease, with special reference to operative procedures and their relationship to recurrence. Tohuku J Exp Med 1982;137:245–251.
14. Bradley LM, Haynes L, Swain SL. IL-7: maintaining T-cell memory and achieving homeostasis. Trends Immunol 2005;26:172–176.
15. Yamazaki M, Yajima T, Tanabe M, Fukui K, Okada E, Okamoto R, Oshima S, Nakamura T, Kanai T, Uehira M, Takeuchi T, Ishikawa H, Hibi T, Watanabe M. Mucosal T cells expressing high level of IL-7 receptor are potential targets for treatment of chronic colitis. J Immunol 2003;171:1556–1563.
16. Okada E, Yamazaki M, Tanabe M, Takeuchi T, Nanno M, Oshima S, Okamoto R, Tsuchiya K, Nakamura T, Kanai T, Hibi T, Watanabe M. IL-7 exacerbates chronic colitis with expansion of memory IL-7R^{high} CD4+ mucosal T cells in mice. Am J Physiol Gastrointest Liver Physiol 2005;288:745–754.
17. Seddon B, Tomlinson P, Zamoyska R. Interleukin 7 and T cell receptor signals regulate homeostasis of CD4 memory cells. Nat Immunol 2003;4:680–686.
18. Totsuka T, Kanai T, Iiyama R, Uraushihara K, Yamazaki M, Okamoto R, Hibi T, Tezuka K, Azuma M, Akiba Yagita H, Okumura K, Watanabe M. Ameliorating effect of anti-ICOS monoclonal antibody in a murine model of chronic colitis. Gastroenterology 2003;124:410–421.
19. Cong Y, Brandwein SL, McCabe RP, Lazenby A, Birkenmeier EH, Sundberg JP, Elson CO. CD4+ T cells reactive to enteric bacterial antigens in spontaneously colitic C3H/HeJBir mice: increased T helper cell type 1 response and ability to transfer disease. J Exp Med 1998;187:855–864.
20. Fagarasan S, Muramatsu M, Suzuki K, Nagaoka H, Hiai H, Honjo T. Critical roles of activation-induced cytidine deaminase in the homeostasis of gut flora. Science 2002;298:1424–1427.
21. Johansson-Lindborm B, Svensson M, Wurbel MA, Malissen B, Marquez G, Agace W. Selective generation of gut tropic T cells in gut-associated lymphoid tissue (GALT): requirement for GALT dendritic cells and adjuvant. J Exp Med 2003;198:963–969.
22. Mora JR, Rosa Bonbo M, Manjunath N, Weninger W, Cavanagh LL, Rosemblatt M, von Andrian UH. Selective imprinting of gut-homing T cells by Peyer's patch dendritic cells. Nature 2003;424:88–93.
23. Namen AE, Lupton S, Hjerrild K, Wignall J, Mochizuki DY, Schmierer A, Mosley B, March CJ, Urdal D, Gillis S. Stimulation of B-cell progenitors by cloned murine interleukin-7. Nature 1988;333:571–573.
24. Tokoyoda K, Egawa T, Sugiyama T, Choi B-II, Nagasawa T. Cellular niches controlling B lymphocyte behavior within bone marrow during development. Immunity 2004;20:707–714.
25. Strober W, Fuss IJ, Blumberg RS. The immunology of mucosal models of inflammation. Annu Rev Immunol 2002;20:495–549.
26. Kuhn R, Lohler J, Rennick D, Rajewsky K, Muller W. Interleukin-10-deficient mice develop chronic enterocolitis. Cell 1993;75:263–274.
27. Cavanagh LL, Bonasio R, Mazo IB, Halin C, van der Velden AW, Cariappa A, Chase C, Russell P, Starnbach MN, Koni PA, Pillai S, Weninger W, von Andrian UH. Activation of bone marrow-resident memory T cells by circulating, antigen-bearing dendritic cells. Nat Immunol 2005;6:1029–1037.
28. Jelley-Gibbs DM, Lepak NM, Yen M, Swain SL. Two distinct stages in the transition from naïve CD4 T cells to effectors, early antigen-dependent and late cytokine-driven expansion and differentiation. J Immunol 2000;165:5017–5026.
29. Garcia-Ojeda ME, Dejbakhsh-Jones S, Weissman IL, Strober S. An alternate pathway for T cell development supported by the bone marrow microenvironment: recapitulation of thymic maturation. J Exp Med 1998;187:1813–1823.
30. Parretta E, Cassese G, Barba P, Santoni A, Guardiola J, Di Rosa F. CD8 cell division maintaining cytotoxic memory occurs predominantly in the bone marrow. J Immunol 2005;174:7654–7664.
31. Becker TC, Coley SM, Wherry EJ, Ahmed R. Bone marrow is a preferred site for homeostatic proliferation of memory CD8 T cells. J Immunol 2005;174:1269–1273.

Received November 8, 2005. Accepted September 14, 2006

Address requests for reprints to: Takanori Kanai, MD, Department of Gastroenterology and Hepatology, Tokyo Medical and Dental University, 1-5-45 Yushima, Bunkyo-ku, Tokyo 113-8519, Japan. e-mail: taka.gast@tmd.ac.jp; fax: (81) 3-5803-0268.

Supported in part by grants-in-aid for Scientific Research, Scientific Research on Priority Areas, Exploratory Research and Creative Scientific Research from the Japanese Ministry of Education, Culture, Sports, Science and Technology; the Japanese Ministry of Health, Labor and Welfare; the Japan Medical Association; the Foundation for Advancement of International Science; Terumo Life Science Foundation; Ohyama Health Foundation; Yakult Bio-Science Foundation; and the Research Fund of Mitsukoshi Health and Welfare Foundation.

The authors are grateful to R. Zamoyska for providing mice and to C. O. Elson for technical advice.

nature
cell biology

Plexin-A1 and its interaction with DAP12 in immune responses and bone homeostasis

Noriko Takegahara[1,12], Hyota Takamatsu[1,12], Toshihiko Toyofuku[1,2], Tohru Tsujimura[3], Tatsusada Okuno[4], Kazunori Yukawa[5], Masayuki Mizui[1], Midori Yamamoto[1], Durbaka V.R. Prasad[1], Kazuhiro Suzuki[1], Masaru Ishii[6], Kenta Terai[7], Masayuki Moriya[4], Yuji Nakatsuji[4], Saburo Sakoda[4], Shintaro Sato[8], Shizuo Akira[8], Kiyoshi Takeda[9], Masanori Inui[10], Toshiyuki Takai[10], Masahito Ikawa[11], Masaru Okabe[11], Atsushi Kumanogoh[1,13] and Hitoshi Kikutani[1,13]

Semaphorins and their receptors have diverse functions in axon guidance, organogenesis, vascularization and/or angiogenesis, oncogenesis and regulation of immune responses[1–11]. The primary receptors for semaphorins are members of the plexin family[2,12–14]. In particular, plexin-A1, together with ligand-binding neuropilins, transduces repulsive axon guidance signals for soluble class III semaphorins[15], whereas plexin-A1 has multiple functions in chick cardiogenesis as a receptor for the transmembrane semaphorin, Sema6D, independent of neuropilins[16]. Additionally, plexin-A1 has been implicated in dendritic cell function in the immune system[17]. However, the role of plexin-A1 *in vivo*, and the mechanisms underlying its pleiotropic functions, remain unclear. Here, we generated *plexin-A1*-deficient (*plexin-A1*$^{-/-}$) mice and identified its important roles, not only in immune responses, but also in bone homeostasis. Furthermore, we show that plexin-A1 associates with the triggering receptor expressed on myeloid cells-2 (Trem-2), linking semaphorin-signalling to the immuno-receptor tyrosine-based activation motif (ITAM)-bearing adaptor protein, DAP12. These findings reveal an unexpected role for plexin-A1 and present a novel signalling mechanism for exerting the pleiotropic functions of semaphorins.

To better understand the role of plexin-A1 *in vivo*, mice deficient in the *plexin-A1* gene were generated by homologous recombination (see Supplementary Information, Fig. S1a, b), and the successful deletion of *plexin-A1* was confirmed by both northern blotting and RT–PCR (see Supplementary Information, Fig. S1c, d). Mice were born with the expected Mendelian ratios from intercrosses of heterozygous mutants and the resulting *plexin-A1*$^{-/-}$ mice were fertile. Apparent abnormalities were not observed by gross macroscopic or histological examination of the embryos (E11.5) or in the brain, kidney, lung, heart, liver and spleen of 4-week-old mice — all tissues in which *plexin-A1*-transcripts are expressed (see Supplementary Information, Fig. S1e, f). These observations strongly suggest the existence of functional redundancy among the plexin family members during embryonic development. However, mutant mice had functional defects in the immune system, as well as morphologic abnormalities in the skeletal tissues. Therefore, the biological functions of plexin-A1 were further investigated with a focus on the immune and skeletal tissues as described below.

Lymphocyte development seemed to be normal in *plexin-A1*$^{-/-}$ mice. No differences in the expression of cell surface phenotype markers, numbers and ratios of T-cells, B-cells, macrophages and dendritic cells in the spleen and thymus were observed between wild-type and *plexin-A1*$^{-/-}$ mice (see Supplementary Information, Fig. S1g). Plexin-A1 is highly expressed in dendritic cells[17], and the influence of *plexin-A1*-deficiency on dendritic cell function was examined. FITC–dextran uptake by dendritic cells, and the appearance of fluorescent dendritic cells in the draining lymph nodes after skin painting with FITC, in *plexin-A1*$^{-/-}$ mice were comparable with those seen in wild-type littermates (Fig. 1a, b). In addition, no significant differences were seen in the expression levels of costimulatory molecules (including CD40, CD80, CD86 and MHC class II) between wild-type and *plexin-A1*$^{-/-}$ dendritic cells (Fig. 1c). However, *plexin-A1*$^{-/-}$

[1]Department of Molecular Immunology and CREST program of JST, Research Institute for Microbial Diseases, Osaka University, 3–1 Yamada-oka, Suita, Osaka 565-0871, Japan. [2]Department of Internal Medicine and Therapeutics, Graduate School of Medicine, Osaka University, 2–2 Yamada-oka, Suita, Osaka 565–0871, Japan. [3]Department of Pathology, Hyogo College of Medicine, Hyogo 663–8501, Japan. [4]Department of Neurology, Graduate School of Medicine, Osaka University, 2–2 Yamada-oka, Suita, Osaka 565–0871, Japan. [5]Department of Physiology II, Wakayama Medical College, 811–1 Kimiidera, Wakayama, Wakayama 641–0012, Japan. [6]Department of Clinical Research, National Osaka Minami Medical Center, Kawachinagano, Osaka 586–8521, Japan. [7]Department of Signal Transduction, Research Institute for Microbial Diseases, Osaka University, 3–1 Yamada-oka, Suita, Osaka 565–0871, Japan. [8]Department of Host Defence, Research Institute for Microbial Diseases, Osaka University, and ERATO, Japan Science and Technology Agency, 3–1 Yamada-oka, Suita, Osaka 565–0871, Japan. [9]Department of Molecular Genetics, Medical Institute for Bioregulation, Kyushu University, 3–1–1 Maidashi, Higashi-ku, Fukuoka 812–8582, Japan. [10]Department of Experimental Immunology, Institute of Development, Aging and Cancer, Tohoku University, Siryo 4–1, Aoba-ku, Sendai 980–8575, Japan and CREST program of JST, Honcho 4–1–8, Kawaguchi, Saitama 332–0012, Japan. [11]Genome Information Research Center, Osaka University, 3–1 Yamada-oka, Suita, Osaka 565–0871, Japan. [12]These authors contributed equally to this work. [13]Correspondence should be addressed to A.K. and H.K. (e-mail: kumanogo@ragtime.biken.osaka-u.ac.jp; kikutani@ragtime.biken.osaka-u.ac.jp)

Received 21 February 2006; accepted 28 April 2006; published online 21 May 2006; DOI: 10.1038/ncb1416

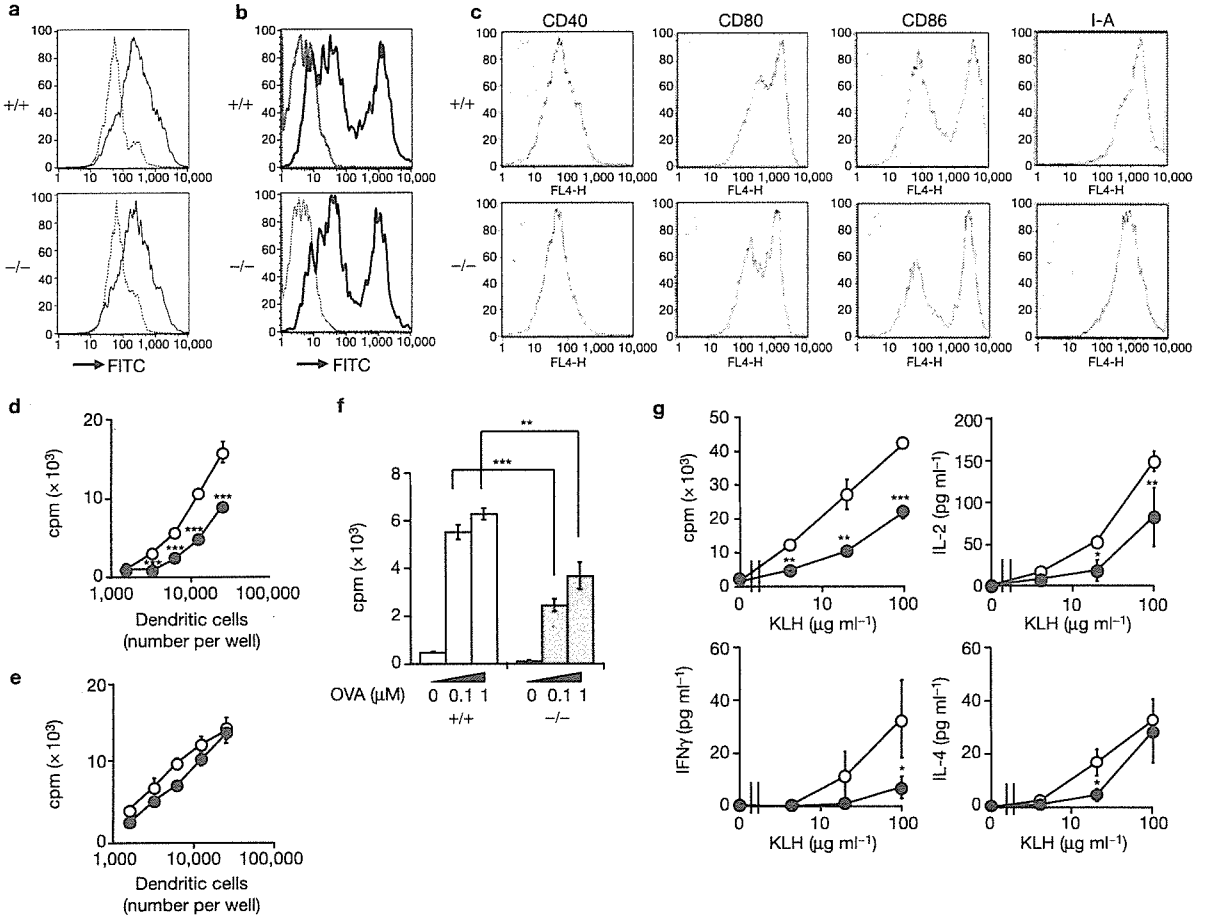

Figure 1 Immunological defects in *plexin-A1*$^{-/-}$ mice. (**a**) *Plexin-A1*$^{-/-}$ dendritic cells take up antigen similar to wild-type cells. BMDCs from wild-type (+/+) or *plexin-A1*$^{-/-}$ (–/–) mice were stained with allophycocyanin (APC)–anti-CD11c and cultured with FITC–dextran at 37 °C (thick lines) or on ice (dotted lines) for 10 min. The CD11c-positive cells were analysed for FL1-fluorescence. (**b**) Normal dendritic cell trafficking to draining lymph nodes in *plexin-A1*$^{-/-}$ mice. Wild-type and *plexin-A1*$^{-/-}$ mice were painted with FITC-isomer on the shaved thorax and abdomen. Cells from the draining lymph nodes were stained with APC–anti-CD11c and CD11c-positive cells were analysed for FL1-fluorescence (thick lines). Cells from mice receiving the carrier solution without FITC were used as controls (shade areas). (**c**) Normal expression of costimulatory molecules in *plexin-A1*$^{-/-}$ dendritic cells. BMDCs from wild-type or *plexin-A1*$^{-/-}$ mice were cultured for 24 h with anti-CD40 and stained with phycoerythrin (PE)–anti-B220, FITC–anti-CD11c and biotin–anti-CD40, -anti-CD80, –anti-CD86 or –anti-I-A (thick lines) plus streptavidin–APC. CD11c-positive–B220-negative cells were analysed. (**d**) Reduced stimulatory activities of *plexin-A1*$^{-/-}$ dendritic cells against allogeneic T-cells. Irradiated splenic dendritic cells derived from wild-type (open circles) or *plexin-A1*$^{-/-}$ (closed circles) mice were cultured with wild-type allogeneic CD4$^+$ T-cells for 48 h. (**e**) Normal mixed lymphocyte reactions (MLRs) between wild-type and *plexin-A1*$^{-/-}$ CD4$^+$ T-cells. Irradiated splenic dendritic cells derived from wild-type mice were cultured with allogeneic wild-type (open circles) or *plexin-A1*$^{-/-}$ (closed circles) CD4$^+$ T-cells for 48 h. Data are the mean ± s.d. of triplicates in **d** and **e**. (**f**) Reduced stimulatory activities of *plexin-A1*$^{-/-}$ dendritic cells against antigen-specific T-cells. Irradiated BMDCs from wild-type (white bars) or *plexin-A1*$^{-/-}$ dendritic cells (grey bars) were cultured with CD62L^{high} CD4$^+$ naïve T cells isolated from ovalbumin (OVA)-TCR transgenic mice[30] for 48 h with or without OVA- peptides. Data are the mean ± s.d. of the triplicates. (**g**) Impaired T-cell priming in *plexin-A1*$^{-/-}$ mice. Wild-type (open circles) and *plexin-A1*$^{-/-}$ mice (closed circles) were immunized with KLH in CFA. Five days later, CD4$^+$ T-cells were prepared from the draining lymph nodes and restimulated with KLH. Data are the mean ± s.d. The results shown in **a**–**g** are representative of five independent experiments. * indicates $P<0.05$, ** indicates $P<0.01$ and *** indicates $P<0.001$. Each value was analysed by Student's *t*-test.

dendritic cells poorly stimulated allogeneic T-cells compared with wild-type dendritic cells (Fig. 1d). In contrast, when CD4$^+$ T-cells from *plexin-A1*$^{-/-}$ mice or wild-type littermates were cultured with allogeneic wild-type dendritic cells, no differences were observed (Fig. 1e), suggesting an important role for dendritic cell-expressed plexin-A1 in stimulating allogeneic T-cells. In addition, the ability of *plexin-A1*$^{-/-}$ dendritic cells to stimulate antigen-specific T cells *in vitro* was also impaired (Fig. 1f). These observations are consistent with previous work of that used RNA interference (RNAi)-targeting of *plexin-A1* (ref. 17) showing that RNAi-mediated knock-down of *plexin-A1* in dendritic cells results in a substantial reduction in T-cell stimulation. Thus, the expression of plexin-A1 by dendritic cells seems essential for normal T-cell stimulation. The generation of antigen-specific T-cells in immunized *plexin-A1*$^{-/-}$ mice was examined next. CD4$^+$ T-cells were prepared from the draining lymph nodes of immunized wild-type or *plexin-A1*$^{-/-}$ mice and antigen-specific T-cell responses were examined *in vitro*. Proliferative responses and cytokine production by CD4$^+$ T-cells were considerably reduced in *plexin-A1*$^{-/-}$ mice (Fig. 1g), demonstrating an important role for plexin-A1 in generating antigen-specific T-cells. In contrast, there were no differences in

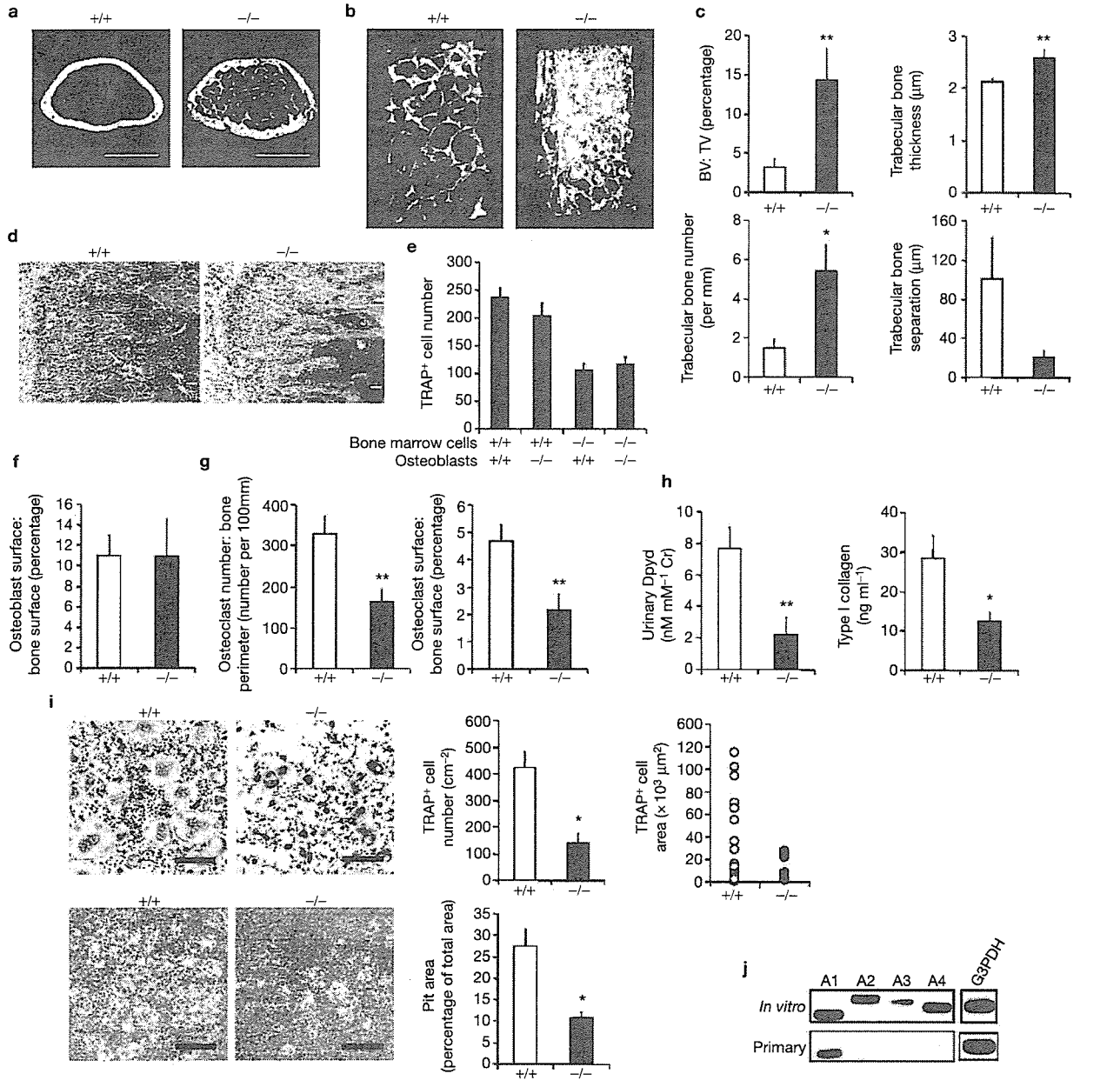

Figure 2 Development of osteopetrosis in *plexin-A1*$^{-/-}$ mice. (**a**, **b**) Microradiographic analysis of the femurs from wild-type (+/+) and *plexin-A1*$^{-/-}$ (−/−) 20-week-old mice. Specimens were scanned using microcomputed tomography. The scale bars represent 1 mm. (**c**) Bone morphometric analyses of femurs from wild-type (n = 5; +/+) and *plexin-A1*$^{-/-}$ (n = 4; −/−) mice. (**d**) Longitudinal sections of wild-type (+/+) and *plexin-A1*$^{-/-}$ (−/−) femurs stained with haematoxylin and eosin. The scale bars represent 50 μm. (**e**, **f**) Normal osteoblast functions in the absence of plexin-A1. Preosteoclasts and calvarial osteoblasts were cocultured in the presence of 1, 25(OH)$_2$ vitamin D$_3$ (VitD$_3$) and prostaglandin E$_2$ (PGE$_2$), and the formation of multinucleated osteoclasts was determined by TRAP staining (**e**). Ratios of osteoblast surface to bone surface in wild-type (n = 4) and *plexin-A1*$^{-/-}$ (n = 4) mice were determined by bone histomorphometry (**f**). (**g**, **h**) Impaired *in vivo* differentiation of osteoclasts in *plexin-A1*$^{-/-}$ mice. Ratios of osteoclast surface to bone surface and osteoclast number per bone perimeter in wild-type (n = 13; +/+) and *plexin-A1*$^{-/-}$ (n = 9; −/−) mice as determined by bone histomorphometry are shown (**g**). Urinary deoxypirydinoline (Dpyd) and serum collagen type I fragment in wild-type (n = 5; +/+) and *plexin-A1*$^{-/-}$ (n = 5; −/−) mice were measured by ELISA (**h**). Cr, creatinine. (**i**) Representative *in vitro* osteoclastogenesis in the absence of plexin-A1. Bone marrow cells derived from wild-type (+/+) or *plexin-A1*$^{-/-}$ (−/−) mice were cultured with M-CSF (10 ng ml^{-1}) and RANKL (50 ng ml^{-1}) and TRAP-positive multinucleated cells (upper) and pit formation (lower) were measured. Mean values ± s.e.m. for each group are shown. The results shown are representative of ten independent experiments. The scale bars represent 200 μm. A single asterisk indicates P<0.05, a double asterisk indicates P<0.01; each value was analysed by Student's t-test. (**j**) Different expression profiles of plexin-A subfamily members between *in vitro* induced and primary isolated osteoclasts. cDNA was prepared from osteoclasts induced by M-CSF plus RANKL (*in vitro*) or from femurs and tibiae of 13-day-old mice (primary). Expression of transcripts of plexin-A1, A2, A3, A4 and G3PDH were determined by PCR using their specific primers.

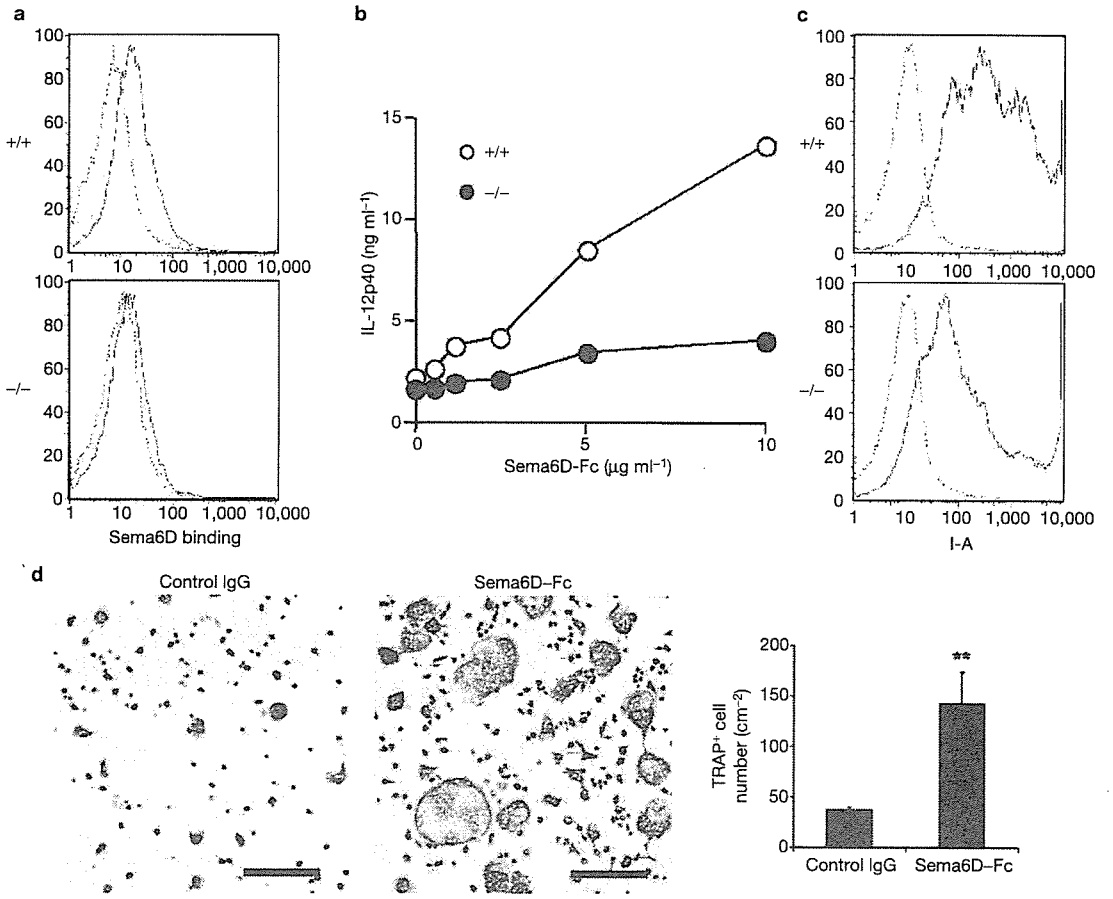

Figure 3 Sema6D promotes dendritic cell activation and osteoclast differentiation. (**a**) Sema6D-binding to dendritic cells. BMDCs from wild-type (+/+) or *plexin-A1*$^{-/-}$ (−/−) mice were cultured with anti-CD40 for 24 h and stained with biotinylated Sema6D-Fc (thick lines) or biotinylated human IgG1 (dotted lines) plus streptavidin–APC. (**b**) Sema6D-induced IL-12 production by dendritic cells. BMDCs from wild-type (open circles) or *plexin-A1*$^{-/-}$ (closed circles) mice were cultured with Sema6D–Fc for 72 h and the production of IL-12p40 was measured by Bio-Plex suspension array system. (**c**) Sema6D-induced upregulation of MHC class II in dendritic cells. BMDCs from wild-type (+/+) or *plexin-A1*$^{-/-}$ (−/−) mice were cultured for 24 h with recombinant soluble Sema6D proteins and stained with PE anti-B220, FITC anti-CD11c and biotin-anti- I-A (thick lines) plus streptavidin–APC. CD11c-positive and B220-negative cells were analysed for the expression of I-A. (**d**) Sema6D promotes osteoclast differentiation. Bone marrow cells from wild-type mice were cultured with M-CSF (10 ng ml^{-1}) and recombinant soluble Sema6D (10 μg ml^{-1}) for 2 days, and cells were further cultured with M-CSF (10 ng ml^{-1}) and a suboptimal dose of RANKL (5 ng ml^{-1}) for 3 days. The number of TRAP-positive cells was measured. The results shown in **a–d** are representative of five independent experiments. The double asterisk indicates $P<0.01$. Each value was analysed with a Student's *t*-test.

the *in vitro* responses of B- and T-cells to mitogenic stimulation between wild-type and *plexin-A1*$^{-/-}$ mice (see Supplementary Information, Fig. S2a–c), consistent with low levels of plexin-A1-expression in B- and T-cells[17] (data not shown).

While isolating bone marrow cells from *plexin-A1*$^{-/-}$ mice, we observed reduced cellularity (by 25 ± 5%) in the long bones of *plexin-A1*$^{-/-}$ animals compared with wild-type littermates. In contrast, cell numbers and lymphocyte populations in the lymphoid organs were similar between mutant and control mice as described (see Supplementary Information, Fig. S1g). This led us to speculate that plexin-A1 may have a previously unknown function in bone homeostasis. Three-dimensional microstructural analyses using high-resolution microcomputed tomography revealed that plexin-A1-deficiency unexpectedly resulted in increased bone mass (Fig. 2a, b and see Supplementary Information, Movie 1 and 2), which was confirmed using bone morphometric analyses (Fig. 2c). Sections of *plexin-A1*$^{-/-}$ long bones had increased trabecular mass compared with wild-type bones (Fig. 2d), indicating the development of osteopetrosis in *plexin-A1*$^{-/-}$ mice. The increased bone mass in *plexin-A1*$^{-/-}$ mice may be a consequence of increased osteoblast function, decreased osteoclast function, or both. To determine the cellular mechanism for the osteopetrosis observed in *plexin-A1*$^{-/-}$ mice, the development and functions of osteoblasts and osteoclasts was examined. *Plexin-A1*$^{-/-}$ osteoblasts promoted the formation of wild-type osteoclasts to the same extent as wild-type osteoblasts (Fig. 2e) and *plexin-A1*$^{-/-}$ osteoblasts isolated from calvarias had no obvious functional differences in the secretion of osteoclastogenic factors, including macrophage-colony stimulating factor (M-CSF) and soluble receptor activator of NF-κB ligand (RANKL), and *in vitro* calcification (data not shown). There were no differences in the levels of osteoblast markers between wild-type and *plexin-A1*$^{-/-}$ mice (see Supplementary Information, Fig. S3a, b). In addition, bone morphometric analysis showed normal ratios of osteoblast surface to bone surface (Fig. 2f). Calcein labelling also showed normal osteoblast activity *in vivo* (see Supplementary Information, Fig. S3c). Collectively, the loss

of plexin-A1 had no apparent influence on osteoblast development and function. In contrast, histological bone morphometric analyses using TRAP-staining showed that *plexin-A1*$^{-/-}$ mice had decreased osteoclast numbers and lower ratios of osteoclast surface to bone surface (Fig. 2g). In addition, *plexin-A1*$^{-/-}$ mice displayed a decrease in deoxypirydinoline (Dpyd) and collagen type I fragments (Fig. 2h), both of which are markers of osteoclast activity and bone resorption, indicating reduced *in vivo* bone turnover by ostoclasts. Consistently, the *in vitro* induction of osteoclasts[18,19] was reduced in the absence of plexin-A1 (Fig. 2i). However, the number of TRAP-positive cells varied between individual mutant mice, and some mutant mice (approximately 40%) exhibited a normal number of TRAP-positive cells *in vitro*. The expression of all plexin-A members was seen in *in vitro* induced osteoclasts (Fig. 2j). It is possible that this variability may be due to the compensatory mechanisms involving other plexin-A family members.

Plexin-A1 is involved in the generation of immune responses and skeletal homeostasis, but the ligands responsible for these effects were unclear. In the nervous system, plexin-A1 associates with neuropilins, functioning as a signal transducing receptor component for class III semaphorins such as Sema3A[2,15,20]. However, recombinant Sema3A neither promoted IL-12 production or costimulatory molecule expression on dendritic cells, nor enhanced osteoclastogenesis *in vitro* (data not shown). Conversely, we previously identified plexin-A1 as a receptor for Sema6D during chick cardiac development[16]. In the immune system, Sema6D is highly expressed in T-cells (see Supplementary Information, Fig. S4a, b), suggesting a role for Sema6D–plexin-A1 interactions in T-cell–dendritic cell cell–cell contacts. We thus examined the effects of soluble recombinant Sema6D on dendritic cell function. Incubation of dendritic cells with recombinant soluble Sema6D[16] induced IL-12 production and upregulation of MHC class II-expression (Fig. 3a–c), although similar effects were not observed in control recombinant Sema4A proteins (see Supplementary Information, Fig. S4c)[8]. In addition, Sema6D is expressed on osteoclasts (see Supplementary Information, Fig. S4b), and soluble recombinant Sema6D promoted substantial osteoclast differentiation *in vitro* (Fig. 3d). Collectively, these results strongly suggest that plexin-A1 is a functional receptor for Sema6D in both the immune and skeletal tissues, as well as during cardiac development in chicks. Consistent with this hypothesis, when *plexin-A1*$^{-/-}$ dendritic cells were incubated with Sema6D, Sema6D binding, IL-12 production and MHC class II upregulation were all considerably reduced (Fig. 3a–c). However, residual Sema6D-binding was observed in *plexin-A1*$^{-/-}$ osteoclast precursors induced *in vitro* (see Supplementary Information, Fig. S4d), indicating that recombinant soluble Sema6D still promoted the *in vitro* induction of osteoclasts in the absence of plexin-A1 (data not shown). As previously described[16], Sema6D can weakly bind other plexin-A subfamily members, such as plexin-A4. The different responsiveness to Sema6D between dendritic cells and osteoclasts in *plexin-A1*$^{-/-}$ mice is likely to be due to the expression of other plexin-A subfamily members in osteoclasts (Fig. 2j and see Supplementary Information, Fig. S4e).

A common mechanism may underlie plexin-A1-function in the immune system and skeletal tissue. Alternatively, these functions may be unrelated. It is noteworthy that plexins utilize different coreceptors to exert a variety of biological effects[2,16,21]. Indeed, plexin-A1 forms a receptor complex with receptor-type tyrosine kinases such as vascular endothelial growth factor receptor 2 (VEGFR2) or Off-track in a region-specific manner during chick cardiac morphogenesis[16]. However, VEGFR2 and Off-track expression was not detected in dendritic cells (data not shown). Therefore, plexin-A1 may associate with other novel coreceptors to exert the functions described here. To better understand the mechanisms by which plexin-A1 affects both the immune system and bone homeostasis, several candidate molecules with putative functions in both dendritic cells and osteoclasts were screened for association with plexin-A1. Using this approach, Trem-2 was found to associate with plexin-A1 (Fig. 4a and see Supplementary Information, Fig. S5a). Trem-2 forms a receptor complex with DAP12, an ITAM-bearing activating adaptor protein, through a positively-charged amino acid in its transmembrane domain[22,23]. Interestingly, Trem-2 and DAP12 have critical roles not only in the development of immune responses but also in bone homeostasis by regulating osteoclast development[24,25]. In COS7 cells transfected with plexin-A1, Trem-2 and DAP12, the association of plexin-A1 with DAP12, in the presence of Trem-2, was observed (Fig. 4b, c), and this was also confirmed in cells stably expressing these proteins and in dendritic cells (Fig. 4d, e). To determine the structural requirements for the association of plexin-A1 and Trem-2, constructs encoding Trem-2 were cotransfected with a series of amino (N)-terminal truncation mutants of plexin-A1. As shown in Fig. 4f, the association of plexin-A1 with Trem-2 was still detected even in the absence of the Sema and plexin–semaphorin–integrin (PSI) domains of plexin-A1, although the association was considerably reduced. However, the association was completely abolished by deletion of the plexin-A1 TIG domain. It thus seems that the plexin-A1 TIG domain is minimally required for the interaction of plexin-A1 with Trem-2.

To determine the role of Trem-2 and DAP12 in semaphorin-mediated signals, a loss of function experiment was performed. RNAi against *Trem-2* reduced the stimulatory activities of Sema6D on dendritic cells (Fig. 4g). Similarly, *DAP12*$^{-/-}$ dendritic cells exhibited considerably reduced responses to Sema6D (Fig. 4h). When RAW264.7 cells expressing plexin-A1, Trem-2 and DAP12 were stimulated with recombinant soluble Sema6D protein, tyrosine phosphorylation of DAP12 was observed (Fig. 4i). Collectively, these results strongly suggest that DAP12 and Trem-2 are functional receptor components for Sema6D.

Plexin-A1 is expressed in a broad range of tissues from embryos to adults (see Supplementary Information, Fig. S1f), and a role for plexin-A1 in axon guidance and cardiac morphogenesis during development has previously been suggested[15,16]. However, this study indicates that the developmental or functional defects of *plexin-A1*$^{-/-}$ mice are primarily restricted to the immune and skeletal tissues. Failure to detect defects in the nervous and cardiovascular systems may be due to compensatory mechanisms by other plexin family members. Additionally, it is possible that the mutant mice have subtle defects that were overlooked in our gross macroscopic and histological analyses. More detailed examination of the mutant mice is required to answer these questions.

Either antigen-uptake or expression levels of costimulatory molecules on *plexin-A1*$^{-/-}$ dendritic cells were comparable with those on wild-type dendritic cells (Fig. 1a–c), indicating that plexin-A1 is not involved in the development of dendritic cells. However, the allogeneic and antigen-specific T-cell stimulatory activities of dendritic cells were impaired in *plexin-A1*$^{-/-}$ mice (Fig. 1d, f), suggesting that the *plexin-A1*-deficiency on dendritic cells is primarily responsible for the impaired ability of dendritic cells to stimulate T-cells. In this context, the reduced stimulatory activities of *plexin-A1*$^{-/-}$ dendritic cells could explain the defective

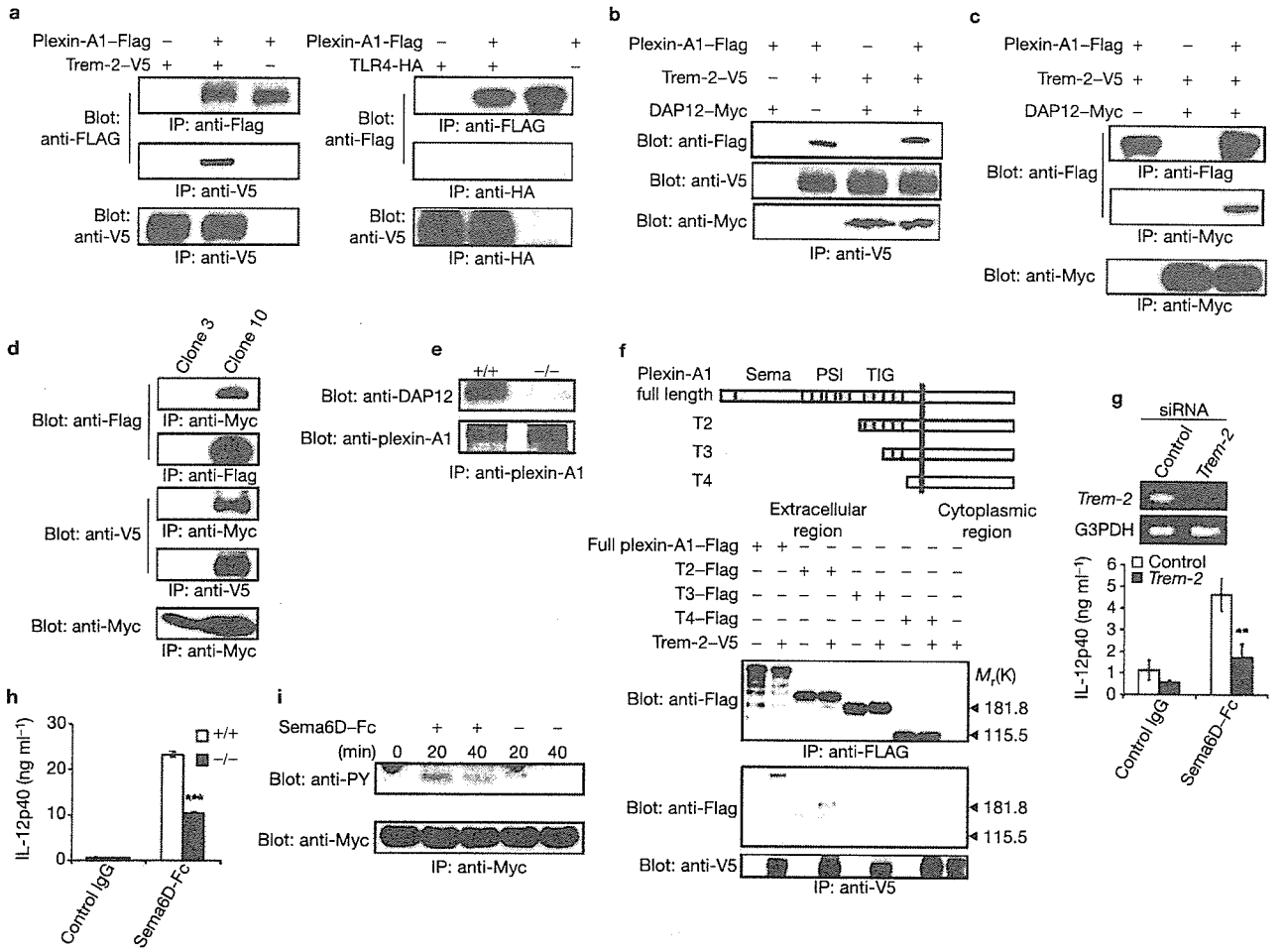

Figure 4 Association of plexin-A1 with Trem-2 and DAP12. (**a**) Association of plexin-A1 with Trem-2. COS7 cells were transfected with plexin-A1 and Trem-2 (left). As a negative control, COS7 cells were transfected with plexin-A1 and TLR4 (right). Cell lysates (1% digitonin) were immunoprecipitated and immunoblotted as indicated. (**b**, **c**) Association of plexin-A1 with DAP12 through Trem-2. COS7 cells were transfected with plexin-A1, Trem-2 or DAP12. Cell lysates (1% digitonin) were immunoprecipitated and immunoblotted as indicated. (**d**) Association of plexin-A1 with Trem-2 and DAP12. Cell lysates of 293T cells stably expressing plexin-A1 (Flag-tagged), Trem-2 (V5-tagged) and DAP12 (Myc-tagged; clone 10) were immunoprecipitated and immunoblotted as indicated. 293T cells stably expressing only DAP12 (Myc-tagged; clone 3) were used as controls. (**e**) Association of plexin-A1 with DAP12 in dendritic cells. Cell lysates of wild-type or *DAP12*$^{-/-}$ dendritic cells were immunoprecipitated and immunoblotted as indicated. (**f**) Plexin-A1 associates with Trem-2 through its TIG domain. The following constructs were used for coprecipitation assays: full-length plexin-A1; plexin-A1–T2 (lacking Sema and PSI domains); plexin-A1–T3 (lacking Sema, PSI and half of the N-terminal TIG domains); and plexin-A1–T4 (lacking Sema, PSI and TIG domains). COS7 cells transfected with the indicated expression vectors were solubilized in 1% digitonin buffer and cell lysates were immunoprecipitated and immunoblotted as indicated. (**g**) Trem-2 is a functional receptor component for Sema6D. BMDCs transfected with siRNA specific for *Trem-2* or non-silencing siRNA were cultured with control IgG or Sema6D-Fc for 72 h. *Trem-2*-expression in RNAi-treated dendritic cells was determined by RT–PCR analysis. (**h**) DAP12 is a functional receptor component for Sema6D. Wild-type (open bars) or *DAP12*$^{-/-}$ BMDCs (filled bars) were cultured with control IgG or Sema6D–Fc for 72 h. IL-12p40 production in the culture supernatants was measured by ELISA. Data are the mean ± s.d. The results shown are representative of three independent experiments. ** indicates $P<0.01$ and *** indicates $P<0.001$. Each value was analysed by Student's *t*-test. (**i**) Sema6D induces DAP12 tyrosine phosphorylation. RAW264.7 cells expressing plexin-A1, Trem-2 and DAP12 (Myc-tagged) were stimulated with Sema6D–Fc (5 μg ml^{-1}). Cell lysates were immunoprecipitated and immunoblotted as indicated. PY: phosphotyrosine; Uncropped scans of the blots in Fig. 4 are shown in Supplementary Information, Fig. S6.

T-cell priming in *plexin-A1*$^{-/-}$ mice. Interestingly, Sema6D is abundantly expressed on T-cells but is downregulated during T helper cell (Th) differentiation (see Supplementary Information, Fig. S4a, b), suggesting the involvement of Sema6D–plexin-A1 interactions in relatively early phases of immune responses through T-cell–dendritic cell contacts. However, the possible involvement of Sema6D–plexin-A1 interactions in effector phases of immune responses cannot be excluded.

The expression of Sema6D was detected not only in *in vitro* induced osteoclasts but also in freshly isolated osteoclasts (see Supplementary Information, Fig. S4b). However, it is noteworthy that, although Sema6D is a transmembrane-type semaphorin, it has been demonstrated that a soluble form of Sema6D is cleaved from the cell surface[16]. Thus, it is possible that Sema6D can function in both autocrine and paracrine manners during osteoclastogenesis. It remains unclear whether the effects of Sema6D are different depending on autocrine versus paracrine stimulation. Also, further studies will be required to determine whether the biological activity of the transmembrane-type Sema6D is functionally different from that of soluble Sema6D.

Our data describe the involvement of plexin-A1, which can associate with DAP12, in both the development of normal immune responses and bone homeostasis. ITAM-mediated signalling through DAP12 has previously been shown to be an important costimulatory signal, not only for the proper development of immune responses, but also for osteoclast differentiation[24–26]. As reported in *DAP12*$^{-/-}$ mice[26], *plexin-A1*$^{-/-}$ mice displayed impaired generation of antigen-specific T-cells, in which they were resistant to the development of experimental autoimmune encephalomyelitis (EAE; see Supplementary Information, Fig. S2d–f). Also in the skeletal tissues, the defects in the *DAP12* gene, as well as the *Trem-2* gene, are known to result in impaired differentiation of osteoclasts[24,25,27,28]. Thus, the association of plexin-A1 with DAP12 may provide costimulatory signals to both dendritic cells and osteoclasts (see Supplementary Information, Fig. S5b, c). However, this association was not relevant to Sema6D-binding to plexin-A1 (Supplementary Information, Fig. S5d, e). We also present evidence that Trem-2 acts as a bridge for the plexin-A1–DAP12 association. Although the expression of other Trem family members was barely detected in dendritic cells and osteoclasts (data not shown)[23], it is possible that other Trem members may be involved in plexin-signals in other cells. Furthermore, not all the functions of plexin-A1 observed here can be explained through its association with Trem-2–DAP12 as *DAP12*$^{-/-}$ dendritic cells displayed weak but substantial responses to Sema6D (Fig. 4h). Indeed, the stimulation of plexin-A1 by recombinant soluble Sema6D proteins induced the activation of Rac, a Rho GTPase[16,29], yet Sema6D-induced Rac activation was not affected in *DAP12*$^{-/-}$ cells (see Supplementary Information, Fig. S5f), suggesting the existence of DAP12-independent signalling pathways through plexin-A1. Further studies will not only clarify the mechanisms of the pleiotropic functions of semaphorins, but also provide potential therapeutic targets for the control of immune and skeletal disorders. □

METHODS

Mice. To construct the *plexin-A1* targeting vector, a 3-kb fragment containing the second exon with the initiation codon. and third exon with the coding sequence of the Sema-domain, was replaced with a neo resistance cassette, and the Herpes simplex virus thymidine kinase (HSV-*TK*) gene was inserted for selection against random integration. The linearized targeting plasmid DNA was transfected into embryonic stem (ES) cells by electroporation. After double selection with G418 and gancyclovir, 96 resistant clones were screened for homologous recombination of the *plexin-A1* targeted allele by PCR and Southern blot analysis as described below. Two clones with homologous recombination were identified and isolated. ES cells from the two independent *plexin-A1* mutant clones were injected separately into blastocysts from C57BL/6 mice. The blastocysts were transferred to pseudopregnant ICR foster mothers and chimeric males were then backcrossed to C57BL/6 or BALB/c females. Heterozygous mice were mated to produce homozygotes. For immunological analysis, heterozygous male mice were backcrossed to C57BL/6 or BALB/c females for five generations. Germline transmission and the genotype of *plexin-A1*-targeted allele were further assayed by Southern blot and PCR analysis. PCR was carried out with 35 cycles of 94 °C for 30 s, 60 °C for 30 s and 72 °C for 60 s. The following oligonucleotide primers were used to identify the rearranged *plexin-A1* locus: primer 1 (5′-AGCACCACACTCACACCCTCTTT-3′) was complementary to genomic DNA that was located in the 3′-untranslated region; primer 2 (5′-TCCTTGATTTTCTCCTTGATGGCC-3′) was complementary to sequences at the 3′-terminus of the second exon; And primer 3 (5′-TCCCTGTCAGAGAAAACCTGGTTT-3′) was complementary to genomic DNA that was located in the untranslated region in the third exon. For Southern blot analysis, genomic DNA from the tails was digested with *BamHI* and subjected to agarose gel electrophoresis. DNA was transferred onto nylon blotting membranes (Hybond N; Amersham Pharmacia, Piscataway, NJ), according to the manufacturer's protocol. Filters were hybridized with radiolabelled probes overnight. Filters were then washed in 0.1× SSC, 0.1% SDS at 65 °C for one hour before autoradiography. For RT–PCR analysis, RNA was isolated from the brain, heart and spleen using RNeasy kits (Qiagen, Hilden, Germany) and treated with DNase I (Invitrogen, Carlsbad, CA) to eliminate genomic DNA. cDNA was synthesized using a SuperScript II cDNA synthesis kit (Invitrogen) and RT–PCR was performed with 35 cycles of 94 °C for 30 s, 60 °C for 30 s and 72 °C for 30 s using the primers (5′-ACATCTACTATGTGTACAGTTTCC-3′) and (5′-AAAAACC ACGGTGCGGCCTTGGGTA-3′). For northern blot analysis, total RNA isolated from the brain was subjected to formaldehyde-containing gel electrophoresis, transferred onto the blotting membrane and hybridized with radiolabelled probes overnight. Mice deficient in DAP12 were previously described[24]. OT-2 transgenic mice were kindly provided by W. R. Heath[30]. Mice were maintained in a specific pathogen-free environment. All experimental procedures were consistent with our institutional guidelines.

***In vitro* assay.** Splenic dendritic cells were isolated from the spleen using MACS (Miltenyi Biotech, Bergisch Gladbach, Germany). The resulting purity was >95% in each experiment. BMDCs were generated from bone marrow progenitors using GM-CSF. For FITC–dextran uptake, BMDCs were stained with allophycocyanin (APC)-conjugated anti-CD11c and incubated with prewarmed medium containing 2 mg ml^{-1} FITC–dextran for 10 min at 37 °C. After washing 3 times with chilled medium, internalised FITC–dextran was measured by FACS. For MLRs, irradiated (3000 rad) splenic dendritic cells were cultured with allogeneic CD4^{+} T-cells (5×10^4 cells per well) for 48 h. To measure cell proliferation, cells were pulsed with 2 μCi of ^{3}H-thymidine for the last 14 h of the culture period.

***In vivo* T-cell responses.** For T-cell priming, mice were immunized with 100 μg keyhole limpet haemocyanin (KLH) in complete Freund's adjuvant (CFA) into the hind footpads[7,8]. Five days after immunization, CD4^{+} T-cells isolated from the draining lymph nodes were stimulated with various concentrations of KLH for 72 h. For proliferation assays, cells were pulsed with 2 μCi ^{3}H-thymidine for the last 14 h. Cytokine production in the culture supernatants was measured using a Bio-Plex suspension array system.

Osteoclast and osteoblast cultures. *In vitro* osteoclastogenesis was performed as previously described[24,25]. In brief, bone marrow progenitor cells derived from wild-type or *plexin-A1*$^{-/-}$ mice were cultured with M-CSF (10 ng ml^{-1}) in α-MEM containing 10% FCS at 5×10^5 cells ml^{-1}. At day 2, cells were harvested and further cultured for 3 days with M-CSF (10 ng ml^{-1}) and RANKL (10 ng ml^{-1}) at 5×10^4 cells ml^{-1} in flat-bottomed 96-well plates. The resulting cells were fixed and stained with tartrate-resistant acid phosphatase using a TRAP-staining kit (Takara, Otsu, Japan). Primary osteoblasts were isolated from neonatal mouse calvaria after sequential digestion with 0.1% collagenase and 0.2% dispase. In coculture experiments, calvarial osteoblasts and stromal cells were cocultured with nonadherent bone marrow cells in medium supplemented with 10 nM 1,25$(OH)_2$-vitamin D_3 and 1 μM prostaglandin E_2.

Analysis of bone phenotype. Histological, histomorphmetric and microradiographic examinations were performed using essentially the same method as previously described[25]. Statistical analysis was performed using Student's *t*-test.

Establishment of stable transfectants. Stable plexin-A1-, Trem-2- and DAP12-expressing 293T cell transfectants were established by introducing Flag-tagged plexin-A1, V5-tagged Trem-2, and Myc-tagged DAP12 expression constructs in a pMC1neo vector using Lipofectamine (Invitrogen) according to the manufacturer's protocol. Transfectants expressing Flag-tagged plexin-A1, V5-tagged Trem-2 and Myc-tagged DAP12 were selected in the presence of G418 and screened using a monoclonal anti-Flag antibody (M2; Sigma, St Louis, MO), monoclonal anti-V5 (Invitrogen) and anti-Myc antibodies (9B11, Cell Signaling Technology, Danvers, MA) and cloned.

RNA interference. Four siRNA sequences specific for mouse *Trem-2* (5′-CCACGGTGCTGCAGGGCAT-3′, 5′-TGACCAAGATGCTGGAGAT-3′, 5′-CGGAATGGGAGCACAGTCA -3′ and 5′-GCACAGTCATCGCAGATGA-3′) were selected (Dharmacon, Piscataway, NJ). All siRNA sequences were synthesized and annealed by the manufacturer (Dharmacon). Transfection was performed using

RNAiFect (Qiagen) according to the manufacturer's protocol. Briefly, dendritic cells were washed and plated in 24-well plates in complete RPMI 1640. Small interference (si) RNAs were incubated with RNAiFect reagent in complete RPMI 1640 at room temperature for 10 min and then added to the dendritic cell culture. After 48 h of incubation, the resulting cells were harvested, washed and used for subsequent experiments. Transfection efficiencies were determined using fluorescein-labelled non-silencing RNA (40–50%).

Immunoprecipitation. Mouse antisera against mouse plexin-A1 were obtained by immunizing *plexin-A1*$^{-/-}$ mice with soluble plexin-A1 protein in CFA and used for immunoblotting. Rabbit antisera against mouse plexin-A1 were used for immunoprecipitation. Wild-type or *DAP12*$^{-/-}$ BMDCs were stimulated with monoclonal anti-CD40 antibodies for 24 h. Cells were solubilized in buffer containing 1% digitonin, 10 mM Tris–HCl, 150 mM NaCl, 0.5 mM PMSF, 5 μg ml^{-1} aprotinin, 5 μg ml^{-1} leupeptin and protease inhibitor cocktail (Nakarai, Kyoto, Japan). Cell lysates were incubated with protein A–Sepharose plus anti-plexin-A1 for 3 h at 4 °C. After five washes with lysis buffer, immunoprecipitates were separated by SDS–PAGE and immunoblotted with anti-DAP12 (ref. 25). Whole cell lysates were immunoblotted with anti-plexin-A1.

Phosphorylation of DAP12. RAW264.7 cells were cotransfected with Flag-tagged plexin-A1, V5-tagged Trem-2 and Myc-tagged DAP12 expression constructs by Lipofectamine (Invitrogen) according to the manufacturer's protocol and incubated for 24 h. Cells were stimulated with 15 μg ml^{-1} Sema6D-Fc after 6 h of serum starvation. At various times, cells were solubilized in buffer containing 1% Nonidet-P40, 10 mM Tris–HCl, 150 mM NaCl, 1 mM EDTA,10 mM Na_3VO_4, 0.5 mM PMSF, 5 μg ml^{-1} aprotinin, 5 μg ml^{-1} leupeptin and protease inhibitor cocktail (Roche, Basel, Switzerland). Cell lysates were incubated with protein G–agarose plus monoclonal anti-Myc antibodies for 3 h at 4 °C. After five washes with lysis buffer, immunoprecipitates were separated by SDS–PAGE and immunoblotted with anti-phosphotyrosine (4G10, Upstate Biotechnology, Charlottesville, VA) or anti-Myc antibodies.

Note: Supplementary Information is available on the Nature Cell Biology website.

ACKNOWLEDGMENTS

We thank K. Kubota for excellent secretarial assistance. We are grateful to H. Murayama and S. Sato for critical discussion and excellent bone analysis, including microCT and histology. We are also grateful to N. Yamamoto, H. Takayanagi, T. Nakano, I. Ishikawa, H. Arase, N. Yamada, T. Kaisho and K. Hoshino for providing materials, critical advice, discussion and encouragement. We also thank T. Yazawa, A. Kawai, J. Yoshida, K Shiozaki, N. Okita, N. Iwami and K. Nakamura for technical support. This study was supported by research grants from the Ministry of Education, Culture, Sports, Science and Technology, Japan and from the Core Research for Evolutional Science and Technology (CREST) program of the Japanese Science and Technology Agency (JST) to A.K. and H.K.

AUTHOR CONTRIBUTIONS

N.T. performed the main experimental work and data analysis for bone analysis. H.T. performed the main experimental work and data analysis for the immune responses. T.T., T.T., T.O., K.Y., M.M., M.Y., D.V.R.P., K.S. and S.S. also performed experimental work. M.I. performed calcium signalling analysis. S.A., K.T., M.I. and M.O. were involved in generating knockout mice. M.I. and T.T. performed the DAP12 analysis. A.K. and H.K. co-organized and performed project planning, data analysis, discussion and writing.

COMPETING FINANCIAL INTERESTS

The authors declare that they have no competing financial interests.

Published online at http://www.nature.com/naturecellbiology/
Reprints and permissions information is available online at http://npg.nature.com/reprintsandpermissions/

1. Tessier-Lavigne, M. & Goodman, S. C. The molecular biology of axon guidance. *Science* **274,** 1123–1133 (1996).
2. Pasterkamp, R. J. & Kolodkin, A. L. Semaphorin junction: making tracks toward neural connectivity. *Curr. Opin. Neurobiol.* **13,** 79–89 (2003).
3. Sekido, Y. *et al.* Human semaphorins A(V) and IV reside in the 3p21.3 small cell lung cancer deletion region and demonstrate distinct expression patterns. *Proc. Natl Acad. Sci. USA* **93,** 4120–4125 (1996).
4. Gu, C. *et al.* Neuropilin-1 conveys semaphorin and VEGF signaling during neural and cardiovascular development. *Dev. Cell* **5,** 45–57 (2003).
5. Toyofuku, T. *et al.* Guidance of myocardial patterning in cardiac development by Sema6D reverse signalling. *Nature Cell Biol.* **6,** 1204–1211 (2004).
6. Kumanogoh, A. *et al.* Identification of CD72 as a lymphocyte receptor for the class IV semaphorin CD100: a novel mechanism for regulating B cell signaling. *Immunity* **13,** 621–631 (2000).
7. Shi, W. *et al.* The class IV semaphorin CD100 plays nonredundant roles in the immune system: defective B and T cell activation in CD100-deficient mice. *Immunity* **13,** 633–642 (2000).
8. Kumanogoh, A. *et al.* Class IV semaphorin Sema4A enhances T-cell activation and interacts with Tim-2. *Nature* **419,** 629–633 (2002).
9. Kumanogoh, A. *et al.* Nonredundant roles of Sema4A in the immune system: defective T cell priming and Th1/Th2 regulation in *Sema4A*-deficient mice. *Immunity* **22,** 305–316 (2005).
10. Kikutani, H. & Kumanogoh, A. Semaphorins in interactions between T cells and antigen-presenting cells. *Nature Rev. Immunol.* **3,** 159–167 (2003).
11. Elhabazi, A., Marie-Cardine, A., Chabbert-de Ponnat, I., Bensussan, A. & Boumsell, L. Structure and function of the immune semaphorin CD100/SEMA4D. *Crit. Rev. Immunol.* **23,** 65–81 (2003).
12. Tamagnone, L. & Comoglio, P. M. Signalling by semaphorin receptors: cell guidance and beyond. *Trends Cell Biol.* **10,** 377–383 (2000).
13. Granziero, L. *et al.* CD100/Plexin-B1 interactions sustain proliferation and survival of normal and leukemic CD5+ B lymphocytes. *Blood* **101,** 1962–1969 (2003).
14. Walzer, T., Galibert, L., Comeau, M. R. & De Smedt, T. Plexin C1 engagement on mouse dendritic cells by viral semaphorin A39R induces actin cytoskeleton rearrangement and inhibits integrin-mediated adhesion and chemokine-induced migration. *J. Immunol.* **174,** 51–59 (2005).
15. Takahashi, T. *et al.* Plexin–neuropilin-1 complexes form functional semaphorin-3A receptors. *Cell* **99,** 59–69 (1999).
16. Toyofuku, T. *et al.* Dual roles of Sema6D in cardiac morphogenesis through region-specific association of its receptor, Plexin-A1, with off-track and vascular endothelial growth factor receptor type 2. *Genes Dev.* **18,** 435–447 (2004).
17. Wong, A. W. *et al.* CIITA-regulated plexin-A1 affects T-cell-dendritic cell interactions. *Nature Immunol.* **4,** 891–898 (2003).
18. Lacey, D. L. *et al.* Osteoprotegerin ligand is a cytokine that regulates osteoclast differentiation and activation. *Cell* **93,** 165–176 (1998).
19. Theill, L. E., Boyle, W. J. & Penninger, J. M. RANK-L and RANK: T cells, bone loss, and mammalian evolution. *Annu. Rev. Immunol.* **20,** 795–823 (2002).
20. Takahashi, T. & Strittmatter, S. M. Plexina1 autoinhibition by the plexin sema domain. *Neuron* **29,** 429–439 (2001).
21. Giordano, S. *et al.* The semaphorin 4D receptor controls invasive growth by coupling with Met. *Nature Cell Biol.* **4,** 720–724 (2002).
22. Lanier, L. L. & Bakker, A. B. The ITAM-bearing transmembrane adaptor DAP12 in lymphoid and myeloid cell function. *Immunol. Today* **21,** 611–614 (2000).
23. Colonna, M. TREMs in the immune system and beyond. *Nature Rev. Immunol.* **3,** 445–453 (2003).
24. Kaifu, T. *et al.* Osteopetrosis and thalamic hypomyelinosis with synaptic degeneration in *DAP12*-deficient mice. *J. Clin. Invest.* **111,** 323–332 (2003).
25. Koga, T. *et al.* Costimulatory signals mediated by the ITAM motif cooperate with RANKL for bone homeostasis. *Nature* **428,** 758–763 (2004).
26. Bakker, A. B. *et al. DAP12*-deficient mice fail to develop autoimmunity due to impaired antigen priming. *Immunity* **13,** 345–353 (2000).
27. Paloneva, J. *et al.* Loss-of-function mutations in *TYROBP (DAP 12)* result in a presenile dementia with bone cysts. *Nature Genet.* **25,** 357–361 (2000).
28. Paloneva, J. *et al.* Mutations in two genes encoding different subunits of a receptor signaling complex result in an identical disease phenotype. *Am. J. Hum. Genet.* **71,** 656–662 (2002).
29. Turner, L. J., Nicholls, S. & Hall, A. The activity of the plexin-A1 receptor is regulated by Rac. *J. Biol. Chem.* **279,** 33199–33205 (2004).
30. Barnden, M. J., Allison, J., Heath, W. R. & Carbone, F. R. Defective TCR expression in transgenic mice constructed using cDNA-based α- and β-chain genes under the control of heterologous regulatory elements. *Immunol. Cell Biol.* **76,** 34–40 (1998).

nature immunology

Detection of pathogenic intestinal bacteria by Toll-like receptor 5 on intestinal CD11c$^+$ lamina propria cells

Satoshi Uematsu[1,7], Myoung Ho Jang[2,7], Nicolas Chevrier[1], Zijin Guo[2], Yutaro Kumagai[1], Masahiro Yamamoto[1], Hiroki Kato[1], Nagako Sougawa[2], Hidenori Matsui[3], Hirotaka Kuwata[4], Hiroaki Hemmi[1], Cevayir Coban[5], Taro Kawai[6], Ken J Ishii[6], Osamu Takeuchi[1,6], Masayuki Miyasaka[2], Kiyoshi Takeda[4] & Shizuo Akira[1,6]

Toll-like receptors (TLRs) recognize distinct microbial components and induce innate immune responses. TLR5 is triggered by bacterial flagellin. Here we generated *Tlr5*$^{-/-}$ mice and assessed TLR5 function *in vivo*. Unlike other TLRs, TLR5 was not expressed on conventional dendritic cells or macrophages. In contrast, TLR5 was expressed mainly on intestinal CD11c$^+$ lamina propria cells (LPCs). CD11c$^+$ LPCs detected pathogenic bacteria and secreted proinflammatory cytokines in a TLR5-dependent way. However, CD11c$^+$ LPCs do not express TLR4 and did not secrete proinflammatory cytokines after exposure to a commensal bacterium. Notably, transport of pathogenic *Salmonella typhimurium* from the intestinal tract to mesenteric lymph nodes was impaired in *Tlr5*$^{-/-}$ mice. These data suggest that CD11c$^+$ LPCs, via TLR5, detect and are used by pathogenic bacteria in the intestinal lumen.

Toll-like receptors (TLRs) recognize a variety of pathogen-associated molecular patterns and induce innate immune responses[1]. TLRs are abundantly expressed on 'professional' antigen-presenting cells such as macrophages and dendritic cells (DCs) and serve as an important link between the innate and adaptive immune responses. So far, 13 TLRs have been identified in mammals. Among the TLR family members, TLR5 was the first to be shown to recognize a protein ligand, bacterial flagellin[2]. Bacterial flagellin is a structural protein that forms the main portion of flagella, which promote bacterial chemotaxis and bacterial adhesion to and invasion of host tissues[3]. Flagellin of *Listeria monocytogenes* and *Salmonella typhimurium* stimulates TLR5 (ref. 4). Thus, TLR5 recognizes flagellin from both Gram-positive and Gram-negative bacteria. *In vitro* studies have shown that TLR5 recognizes the conserved domain in flagellin monomers and triggers proinflammatory as well as adaptive immune responses[5]. In addition, TLR5 is expressed on the basolateral surface of intestinal epithelial cells and is thought to be key in the recognition of invasive flagellated bacteria at the mucosal surface[4]. When exposed to flagellin, human intestinal epithelial cell lines produce chemokines that induce subsequent migration of immature DCs[6]. There is high expression of TLR5 in the human lung[7], and a correlation between a common human TLR5 polymorphism and susceptibility to legionellosis has been identified[8]. Although accumulating evidence suggests that TLR5 is an important sensor for flagellated pathogens, the *in vivo* function of TLR5 is yet to be elucidated.

Here we generated *Tlr5*$^{-/-}$ mice and examined the function of TLR5 *in vivo* in the intestine. We confirmed that flagellin is a natural ligand for TLR5. Although it is known that *in vivo* administration of flagellin induces inflammatory cytokine production, it remains unclear which cell populations produce those cytokines. Because it is known that there is high expression of TLR5 in the intestine, we first isolated and examined intestinal epithelial cells (IECs). Unexpectedly, TLR5 expression in IECs was much lower than that in the whole intestine. Consistent with that, IECs did not produce inflammatory cytokines in response to flagellin. Using a new method for isolating intestinal lamina propria cells (LPCs)[9], we found that CD11c$^+$ LPCs 'preferentially' expressed TLR5 and produced inflammatory cytokines after exposure to flagellin. CD11c$^+$ LPCs sensed pathogenic flagellated bacteria via TLR5 and induced inflammatory responses. In contrast, CD11c$^+$ LPCs do not express TLR4 and did not produce proinflammatory cytokines in response to a commensal bacterium. Although TLR5 initially induced host defenses against flagellated bacteria, *Tlr5*$^{-/-}$ mice were resistant to oral *S. typhimurium* infection. The transport of *S. typhimurium* from the intestinal tract to the mesenteric

[1]Department of Host Defense, Research Institute for Microbial Diseases, Osaka University, Suita Osaka 565-0871, Japan. [2]Laboratory of Immunodynamics, Department of Microbiology and Immunology, Osaka University Graduate School of Medicine (C8), 2-2, Yamada-oka, Suita, 565-0871, Japan. [3]Laboratory of Immunoregulation, Kitasato Institute for Life Sciences and Graduate School of Infection, Control Sciences, Kitasato University, 5-9-1 Shirokane, Minato-ku, Tokyo 108-8641, Japan. [4]Department of Molecular Genetics, Medical Institute of Bioregulation, Kyushu University, 3-1-1 Maidashi, Higashi-ku, Fukuoka 812-8582, Japan. [5]21st Century COE, Combined Program on Microbiology and Immunology, Osaka University, 3-1 Yamada-oka, Suita Osaka 565-0871, Japan. [6]ERATO, Japan Science and Technology Corporation, 3-1 Yamada-oka, Suita Osaka 565-0871, Japan. [7]These authors contributed equally to this work. Correspondence should be addressed to S.A. (sakira@biken.osaka-u.ac.jp).

Received 28 March; accepted 13 June; published online 9 July 2006; doi:10.1038/ni1362

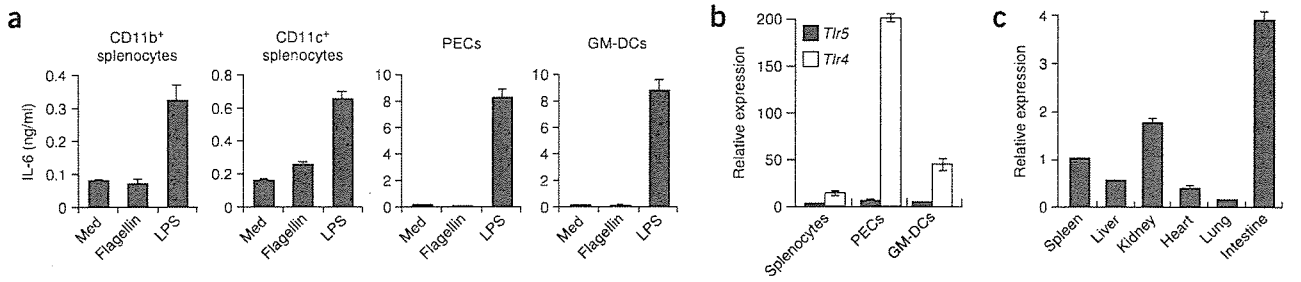

Figure 1 Macrophages and conventional DCs are hyporesponsive to flagellin. (**a**) Enzyme-linked immunosorbent assay of IL-6 production by splenic CD11b$^+$ and CD11c$^+$ cells, GM-DCs and peritoneal macrophages (PECs) from C57BL/6 mice. Cells were cultured with medium only (Med), flagellin (1 μg/ml) or LPS (100 ng/ml). (**b,c**) Quantitative real-time PCR of *Tlr5* and *Tlr4* expression in various cell types (**b**) or organs (**c**) of C57BL/6 mice. Data are mean ± s.d. of triplicate samples from one representative of three independent experiments.

lymph nodes (MLNs) was impaired in *Tlr5*$^{-/-}$ mice. These results suggest that TLR5$^+$CD11c$^+$ LPCs detect and can be used by pathogenic bacteria in the intestine.

RESULTS

Flagellin is a natural ligand for TLR5

To elucidate the physiological function of TLR5, we generated *Tlr5*$^{-/-}$ mice by gene targeting. Mouse *Tlr5* consists of one exon. We constructed the targeting vector to allow insertion of a neomycin-resistance gene cassette into that exon (**Supplementary Fig. 1**). We microinjected two correctly targeted embryonic stem clones into C57BL/6 blastcysts to generate chimeric mice. We crossed chimeric male mice with C57BL/6 female mice and monitored transmission of the mutated allele by Southern blot analysis (**Supplementary Fig. 1**). We then interbred heterozygous mice to produce offspring carrying the null mutation of *Tlr5*. *Tlr5*$^{-/-}$ mice were born at the expected mendelian ratio and showed no developmental abnormalities. To confirm the disruption of *Tlr5*, we analyzed total intestinal RNA from *Tlr5*$^{+/+}$ and *Tlr5*$^{-/-}$ mice by RNA blot and detected no *Tlr5* transcripts in *Tlr5*$^{-/-}$ intestinal RNA (**Supplementary Fig. 1**).

To assess the involvement of TLR5 in the systemic production of proinflammatory cytokines in response to flagellin, we measured the concentrations of interleukin 6 (IL-6) and IL-12p40 in sera of *Tlr5*$^{+/+}$ and *Tlr5*$^{-/-}$ mice at various time points after intraperitoneal injection of purified flagellin. Although IL-6 and IL-12p40 concentrations in the serum increased within 2 h of injection in *Tlr5*$^{+/+}$ mice, their concentrations remained low even at 4 h after injection in *Tlr5*$^{-/-}$ mice (**Supplementary Fig. 1**). These results confirmed that flagellin is a natural ligand for TLR5.

Immune cell responses to flagellin

We next analyzed flagellin-mediated immune responses in macrophages and conventional DCs. We isolated CD11b$^+$ or CD11c$^+$ splenocytes, peritoneal macrophages and granulocyte-macrophage colony stimulating factor–induced bone marrow–derived DCs (GM-DCs) from *Tlr5*$^{+/+}$ mice, stimulated these cells with flagellin or the TLR4 ligand lipopolysaccharide (LPS) and measured IL-6 concentrations in cell culture supernatants (**Fig. 1a**). All cell types produced IL-6 after stimulation with LPS, but IL-6 production was not induced by stimulation with flagellin. In agreement with those results, splenocytes, peritoneal macrophages and GM-DCs had high expression of *Tlr4* but not *Tlr5* mRNA, as determined by quantitative real-time PCR (**Fig. 1b**). To identify the tissues involved in flagellin-induced production of proinflammatory cytokines, we measured *Tlr5* mRNA in the spleen, liver, kidney, heart, lung and intestine by quantitative real-time PCR and found that intestine had the highest expression of *Tlr5* mRNA (**Fig. 1c**).

TLR5 expression is confined to the basolateral surface of IECs[4]. To examine TLR5-mediated inflammatory responses in IECs, we isolated IECs from *Tlr5*$^{+/+}$ and *Tlr5*$^{-/-}$ mice, stimulated them with flagellin and used cDNA microarray to examine the profile of genes induced by TLR5 stimulation (**Fig. 2**). It has been reported that flagellin induces expression of genes encoding some chemokines (such as IL-8 and CCL20) in human IEC lines[6,10]. Our analyses showed flagellin-induced expression of some genes encoding proteins involved in immune responses, such as defensin-β3, CD86, killer cell lectin-like receptor subfamily A member 6, complement component 8α and

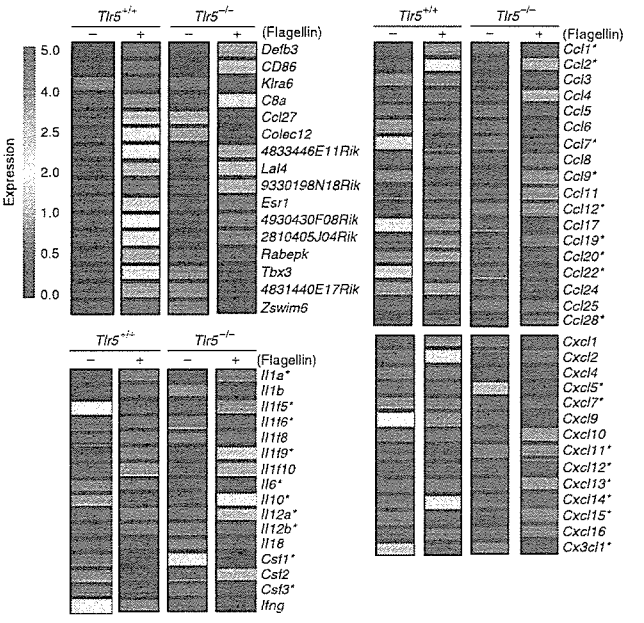

Figure 2 Gene expression induced by flagellin stimulation in IECs. Microarray analysis of IECs from *Tlr5*$^{+/+}$ and *Tlr5*$^{-/-}$ mice stimulated with medium alone (–) or 1 μg/ml of flagellin (+). *, genes judged as being statistically undetectable at all time points. There is flagellin-induced expression of the genes encoding defensin-β3 (*Defb3*), CD86 (*Cd86*), killer cell lectin-like receptor subfamily A member 6 (*Klra6*), complement component 8α (*C8a*) and chemokine (C-C motif) ligand 27 (*Ccl27*) in *Tlr5*$^{+/+}$ but not *Tlr5*$^{-/-}$ IECs. Data are representative of three independent experiments.

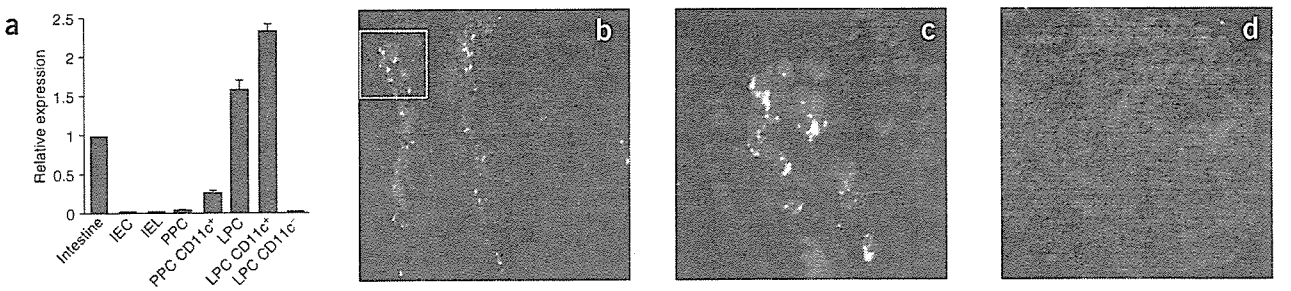

Figure 3 TLR5 is highly expressed on CD11c$^+$ LPCs. (**a**) Quantitative real-time PCR of *Tlr5* expression by the intestine (far left) and by various cell types of C57BL/6 mice. IEL, intestinal epithelial lymphocyte. Data are mean ± s.d. of triplicate samples from one representative of three independent experiments. (**b–d**) Confocal microscopy of frozen tissue sections of small intestine (**b,c**) and Peyer's patch (**d**) of C57BL/6 mice, fixed and stained with antibodies specific for CD11c (red) and TLR5 (green). Image in **c** is an enlargement of the boxed area in **b**. Original magnification ×400 (**b,d**) and ×1,000 (**c**). Data are from one of three representative experiments.

chemokine (C-C motif) ligand 27 in *Tlr5*$^{+/+}$ but not *Tlr5*$^{-/-}$ IECs. However, most genes encoding chemokines were not induced by flagellin, even in *Tlr5*$^{+/+}$ IECs, and flagellin did not induce the expression of any genes encoding proinflammatory cytokines in *Tlr5*$^{+/+}$ IECs. We confirmed that *Tlr5*$^{+/+}$ IECs did not produce proinflammatory cytokine protein after flagellin stimulation (data not shown). There was much less *Tlr5* mRNA in IECs than in the entire small intestine (**Fig. 3a**).

Because TLR5 expression was low in IECs but high in the entire small intestine, we hypothesized that TLR5 must be 'preferentially' expressed in other intestinal cell types. We measured *Tlr5* mRNA in Peyer's patch cells (PPCs), intestinal epithelial lymphocytes and LPCs (**Fig. 3a**). There was high expression of *Tlr5* mRNA in LPCs, but *Tlr5* mRNA expression in intestinal epithelial lymphocytes and PPCs was lower than that in the entire small intestine. DCs are a dominant antigen-presenting cell in the lamina propria of mouse small bowel[11]. Therefore, we separated CD11c$^+$ cells from LPCs and PPCs and measured expression of *Tlr5* mRNA. We detected considerable *Tlr5* mRNA in CD11c$^+$ LPCs but not CD11c$^-$ LPCs. CD11c$^+$ PPCs had less *Tlr5* mRNA than did CD11c$^+$ LPCs. Next we examined the localization of TLR5 protein in the small intestine by immunohistochemistry. In agreement with the mRNA expression data, there was high expression of TLR5 on intestinal CD11c$^+$ LPCs (**Fig. 3b,c**) but not on PPCs (**Fig. 3d**). Thus, TLR5 is expressed specifically on CD11c$^+$ LPCs in the small intestine.

Next we assessed the effect of flagellin stimulation on CD11c$^+$ LPCs. *Tlr5*$^{+/+}$ but not *Tlr5*$^{-/-}$ CD11c$^+$ LPCs produced IL-6 and IL-12p40 in response to flagellin (**Fig. 4**, top). However, CD11c$^+$ LPCs did not produce large amounts of tumor necrosis factor after stimulation with flagellin and failed to produce any cytokines after LPS stimulation.

Antigen-presenting cells in Peyer's patches have been extensively characterized[12]. Peyer's patches contain unusual subsets of DCs that are important in the generation of regulatory T cells and the induction of oral tolerance[12,13]. These Peyer's patch DCs produce IL-10 in response to inflammatory stimulations such as LPS[14]. Consistent with their low expression of *Tlr5* mRNA (**Fig. 3a**), CD11c$^+$ PPCs did not produce inflammatory cytokines after stimulation with flagellin (**Fig. 4**, bottom). However, CD11c$^+$ PPCs produced IL-6 and IL-10 in response to LPS. In contrast, neither *Tlr5*$^{+/+}$ nor *Tlr5*$^{-/-}$ CD11c$^+$ LPCs produced IL-10 in response to flagellin, suggesting that in CD11c$^+$ LPCs, TLR5 signaling induces inflammatory responses but not tolerance (**Fig. 4**).

To comprehensively examine TLR5-mediated innate immune responses in the small intestine, we obtained RNA from *Tlr5*$^{+/+}$ and *Tlr5*$^{-/-}$ LPCs stimulated for 4 h with flagellin and hybridized the RNA to cDNA microarrays (**Fig. 5**). Several transcripts were substantially upregulated at 4 h after flagellin stimulation in *Tlr5*$^{+/+}$ but not *Tlr5*$^{-/-}$ LPCs. These included genes encoding proinflammatory molecules such as cytokines, cytokine receptors, chemokines, signaling molecules, prostanoids, prostanoid synthetase and secretary antimicrobial peptides (**Fig. 5**, top). Genes associated with cellular adhesion,

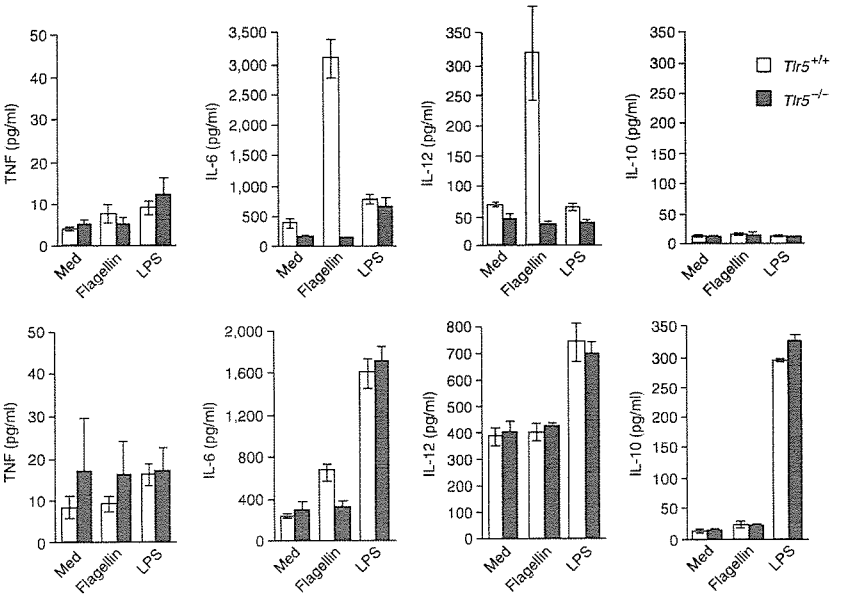

Figure 4 TLR5-mediated CD11c$^+$ LPC cytokine production. Enzyme-linked immunosorbent assay of cytokine production by CD11c$^+$ LPCs (top) and PPCs (bottom) from *Tlr5*$^{+/+}$ and *Tlr5*$^{-/-}$ mice. Cells were cultured with medium only, flagellin (1 μg/ml) or LPS (100 ng/ml). Data are mean ± s.d. of triplicate samples from one representative of three independent experiments.

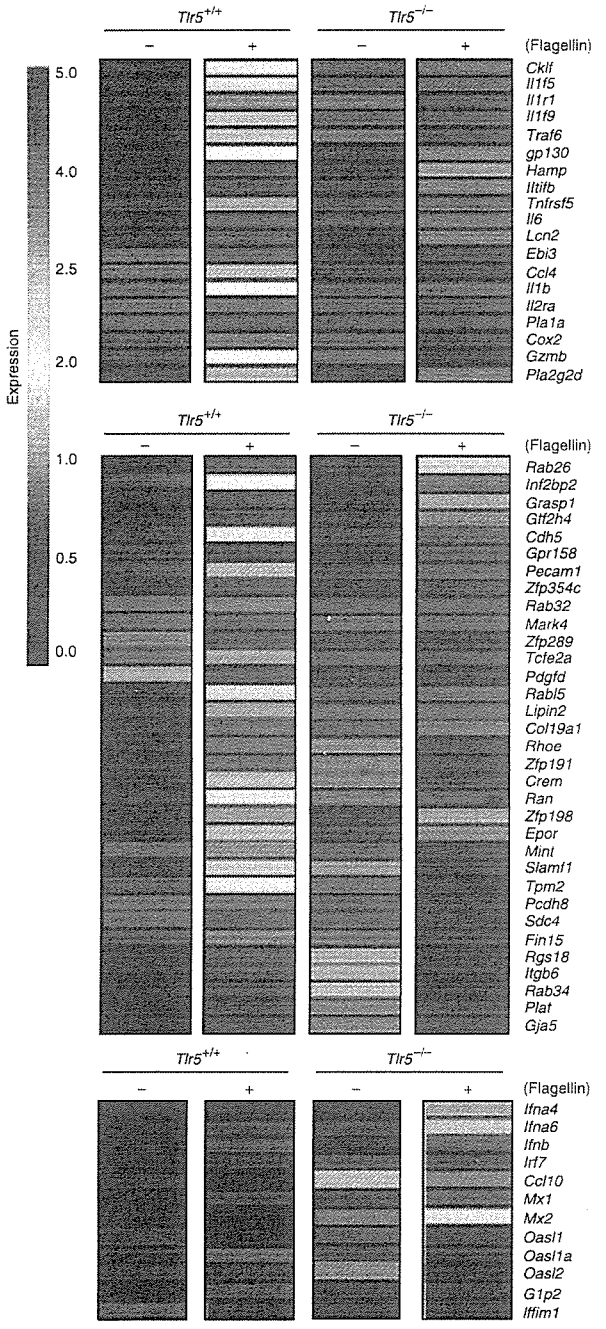

Figure 5 Flagellin-induced gene expression in CD11c$^+$ LPCs. Microarray analysis of CD11c$^+$ LPCs from *Tlr5*$^{+/+}$ and *Tlr5*$^{-/-}$ mice left unstimulated (–) or stimulated with 1 μg/ml of flagellin (+). Upregulated genes encode cytokines (*Il6, Il1f5, Il1f9, Il1b, Ebi3* and *Iltifb*), cytokine receptors (*Tnfrsf5, Il1r1* and *Il2ra*), chemokines (*Cklf* and *Ccl4*), signaling molecules (*Traf6* and *gp130*), prostanoids (*Pla1a* and *Pla2g2d*), prostanoid synthetase (*Cox2*) and secretary antimicrobial peptides (*Hamp, Lcn* and *Gzmb*; top), as well as molecules associated with cellular adhesion, cytoskeletal organization, intracellular transport, vesicle fusion and transcription (middle). Data are representative of three independent experiments.

cytoskeletal organization, intracellular transport, vesicle fusion and transcription were also upregulated by flagellin stimulation (**Fig. 5**, middle). In contrast, interferon and interferon-inducible genes were not induced in response to flagellin in either *Tlr5*$^{+/+}$ or *Tlr5*$^{-/-}$ LPCs (**Fig. 5**, bottom).

CD11c$^+$ LPCs detect pathogenic bacteria via TLR5

CD11c$^+$ LPCs produced IL-6 and IL-12p40 in response to flagellin but not LPS stimulation. CD11c$^+$ LPCs produced similar amounts of IL-6 when stimulated through TLR2 or TLR9 (**Supplementary Fig. 2** online), suggesting that LPS signaling is suppressed specifically in CD11c$^+$ LPCs. Therefore, we measured TLR4 and TLR5 in CD11c$^+$ LPCs and CD11c$^+$ splenic cells (SPCs; **Fig. 6a**). *Tlr4* expression was high and *Tlr5* expression was low in CD11c$^+$ SPCs. In contrast, *Tlr4* expression was low and *Tlr5* expression was high in CD11c$^+$ LPCs.

As CD11c$^+$ LPCs and SPCs had different expression profiles for TLR4 and TLR5, we assessed their responses to commensal and pathogenic bacteria. We isolated CD11c$^+$ LPCs and CD11c$^+$ SPCs from wild-type, *Tlr4*$^{-/-}$ and *Tlr5*$^{-/-}$ mice and measured IL-6 production induced by stimulation with heat-killed commensal Gram-negative bacteria (*Enterobacter cloacae*) and pathogenic Gram-negative bacteria (*S. typhimurium*; **Fig. 6b**). Wild type and *Tlr5*$^{-/-}$ CD11c$^+$ SPCs produced copious IL-6 in response to both *E. cloacae* and *S. typhimurium*. However, *Tlr4*$^{-/-}$ CD11c$^+$ SPCs produced less IL-6 than did wild-type or *Tlr5*$^{-/-}$ CD11c$^+$ SPCs, suggesting that CD11c$^+$ SPCs induce innate immune responses to Gram-negative bacteria mainly via TLR4. Wild-type and *Tlr4*$^{-/-}$ CD11c$^+$ LPCs produced copious IL-6 in response to *S. typhimurium*. In contrast, *Tlr5*$^{-/-}$ CD11c$^+$ LPCs produced little IL-6 after stimulation with *S. typhimurium*. We further assessed the response of CD11c$^+$ LPCs with a mutant strain of *S. typhimurium* that lacks the *fliA* gene and therefore does not produce flagella[15]. Wild-type and *Tlr5*$^{-/-}$ CD11c$^+$ LPCs were hyporesponsive to this *fliA* mutant (compared with their response to wild-type *S. typhimurium*), suggesting that CD11c$^+$ LPCs induce immune responses after recognizing flagellin of *S. typhimurium*. Unlike wild-type CD11c$^+$ SPCs, wild-type CD11c$^+$ LPCs produced a relatively small amount of IL-6 after stimulation with *E. cloacae*. These data suggest that CD11c$^+$ LPCs detect pathogenic flagellated bacteria and induce innate immune responses via TLR5.

S. typhimurium uses TLR5 for systemic infection

To investigate whether TLR5 has a specific function in fighting bacterial infection in the intestine, we orally infected *Tlr5*$^{+/+}$ and *Tlr5*$^{-/-}$ mice with *S. typhimurium*. Unexpectedly, when assessed on a mixed genetic background (C56BL/6 × 129Sv, F2), all *Tlr5*$^{-/-}$ mice survived a dose of *S. typhymurium* that was lethal for *Tlr5*$^{+/+}$ mice (**Fig. 7a**, left). Next we assessed the resistance of *Tlr5*$^{-/-}$ mice backcrossed onto the C57BL/6 genetic background. Although wild-type C57BL/6 mice are resistant to oral *S. typhymurium* infection, *Tlr5*$^{-/-}$ C57BL/6 mice background were significantly more resistant, even at an extremely high dose (5×10^8 bacteria; **Fig. 7a**, right). These results indicate that *Tlr5*$^{-/-}$ mice were resistant regardless of their genetic background. When we challenged mice with *S. typhimurium* by intraperitoneal injection, we noted no significant difference in the survival of *Tlr5*$^{+/+}$ and *Tlr5*$^{-/-}$ mice (**Fig. 7b**). Furthermore, we recovered fewer bacteria from the livers and spleens of *Tlr5*$^{-/-}$ mice than *Tlr5*$^{+/+}$ mice 4 d after oral infection (**Fig. 7c**). At 48 h after oral infection, *Tlr5*$^{+/+}$ and *Tlr5*$^{-/-}$ mice had the same number of *S. typhimurium* in Peyer's patches and LPCs. However, *Tlr5*$^{-/-}$ mice had fewer bacteria in MLNs than did *Tlr5*$^{+/+}$ mice (**Fig. 7d**). In addition, the proportion of *S. typhimurium*–laden CD11c$^+$ cells in MLNs of *Tlr5*$^{-/-}$ mice was smaller than that in *Tlr5*$^{+/+}$ mice (**Supplementary Fig. 3** online). To further determine whether the transport

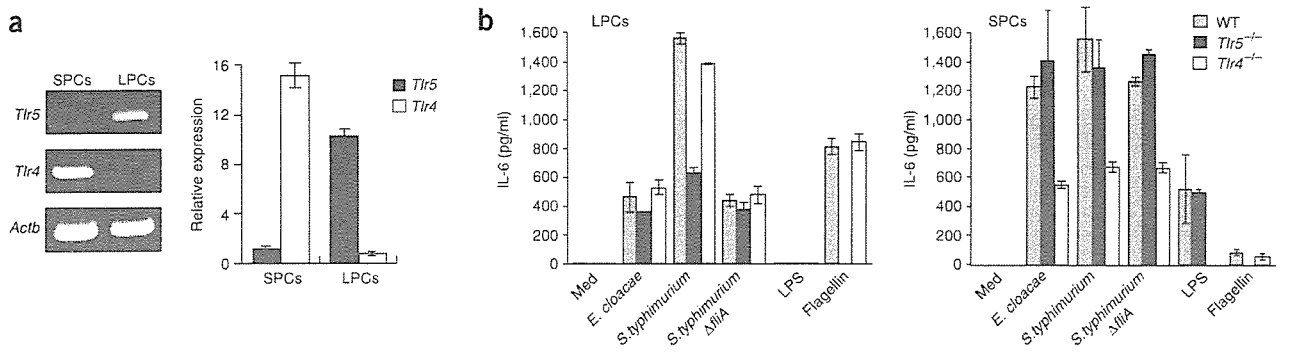

Figure 6 CD11c$^+$ LPCs detect pathogenic bacteria via TLR5. (**a**) Quantitative real-time PCR of *Tlr5* and *Tlr4* expression in CD11c$^+$ SPCs and CD11c$^+$ LPCs of C57BL/6 mice. *Actb* encodes β-actin (loading control). Graphed data are mean ± s.d. of triplicate samples from one representative of three independent experiments. (**b**) Enzyme-linked immunosorbent assay of cytokine production by CD11c$^+$ SPCs and CD11c$^+$ LPCs from wild-type (WT), *Tlr4*$^{-/-}$ and *Tlr5*$^{-/-}$ mice, cultured with medium along (Med) or various stimuli (horizontal axes). Δ*fliA*, mutant strain lacking *fliA*. Data are mean ± s.d. of triplicate samples from one representative of three independent experiments.

of *S. typhimurium* from intestinal tract to MLNs was impaired in *Tlr5*$^{-/-}$ mice, we challenged *Tlr5*$^{+/+}$ and *Tlr5*$^{-/-}$ mice in a surgically isolated intestinal loop with *S. typhimurium* expressing green fluorescent protein (**Supplementary Fig. 4** online). We collected MLNs 24 h after infection. Staining showed that *Tlr5*$^{-/-}$ mice had fewer *S. typhimurium*–laden CD11c$^+$ cells (one to two cells per longitudinal slice of MLN) than did *Tlr5*$^{+/+}$ mice (about ten cells per longitudinal slice of MLN). Furthermore, no cells except CD11c$^+$ cells contained *S. typhimurium* in the infected MLNs. Thus, the impairment of transport of *S. typhimurium* from the intestinal tract to MLNs may lead to a delay in the establishment of systemic infection in *Tlr5*$^{-/-}$ mice.

DISCUSSION

Although TLR5 has been identified as a receptor of flagellin *in vitro*, its *in vivo* function has remained unclear. Addressing the function of TLR5 in innate immunity has been difficult, because unlike other TLR family members, TLR5 is not expressed in mouse spleen cells, peritoneal macrophages or GM-DCs. Using a new method of isolating LPCs with high viability[9], we found that TLR5 is specifically expressed on CD11c$^+$ LPCs in mouse intestine. Although it has long been known that DCs are present in the lamina propria under the villus epithelium and take up antigens from the intestine[16], their functions and properties in the intestine were unknown. CD11c$^+$ LPCs elicited the secretion of various mediators, including inflammatory cytokines, chemokines, antimicrobial peptides and tissue remodeling kinases, in response to flagellin. Thus, we have shown here that immune responses are induced in CD11c$^+$ LPCs via TLR5.

Two points regarding the function of CD11c$^+$ LPCs in relation to TLR5 came to light as a result of our analyses. One was the cytokine profile of CD11c$^+$ LPCs stimulated with flagellin. The gut is continuously exposed to food antigens and many commensal bacteria. Tolerance to beneficial antigens seems to be controlled by mucosal DCs[17]. These DCs stimulate the activity of regulatory T cells, which are potent suppressors of T cell responses. A CD11c^{lo}CD45RB^{hi} DC subset that produces IL-10 has been shown to specifically promote suppressive functions in regulatory T cells[14]. Peyer's patches contain DCs that produce IL-10 after inflammatory stimulation and thereby promote oral tolerance[12,13]. Whereas CD11c$^+$ PPCs induced IL-10 in response to LPS, flagellin-stimulated CD11c$^+$ LPCs did not produce IL-10, but instead produced IL-6 and IL-12, suggesting that CD11c$^+$ LPCs have a tendency to induce inflammatory responses rather than tolerance when stimulated with flagellin. However, it has been

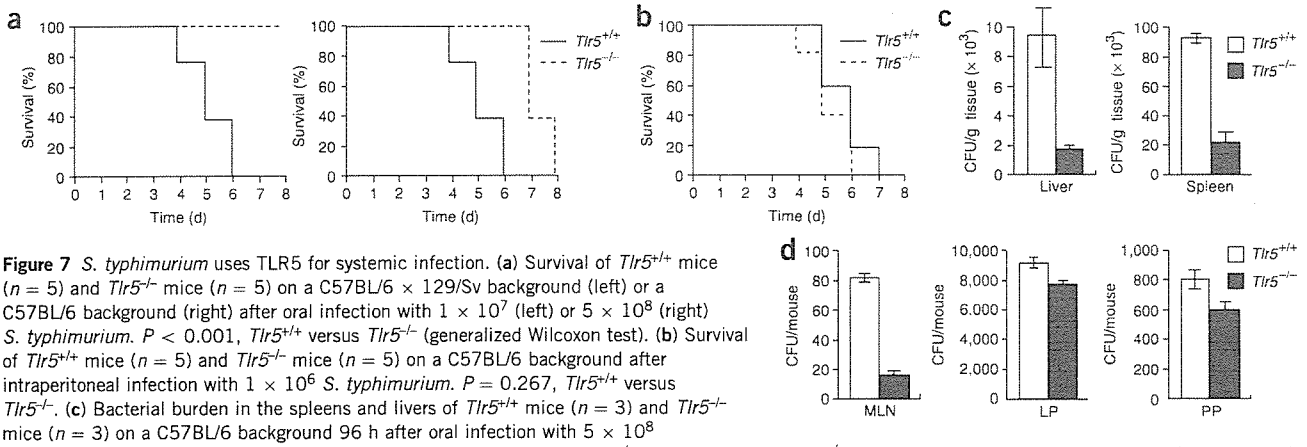

Figure 7 *S. typhimurium* uses TLR5 for systemic infection. (**a**) Survival of *Tlr5*$^{+/+}$ mice ($n = 5$) and *Tlr5*$^{-/-}$ mice ($n = 5$) on a C57BL/6 × 129/Sv background (left) or a C57BL/6 background (right) after oral infection with 1×10^7 (left) or 5×10^8 (right) *S. typhimurium*. $P < 0.001$, *Tlr5*$^{+/+}$ versus *Tlr5*$^{-/-}$ (generalized Wilcoxon test). (**b**) Survival of *Tlr5*$^{+/+}$ mice ($n = 5$) and *Tlr5*$^{-/-}$ mice ($n = 5$) on a C57BL/6 background after intraperitoneal infection with 1×10^6 *S. typhimurium*. $P = 0.267$, *Tlr5*$^{+/+}$ versus *Tlr5*$^{-/-}$. (**c**) Bacterial burden in the spleens and livers of *Tlr5*$^{+/+}$ mice ($n = 3$) and *Tlr5*$^{-/-}$ mice ($n = 3$) on a C57BL/6 background 96 h after oral infection with 5×10^8 *S. typhimurium*. (**d**) Bacterial burden in the MLNs, PPCs and LPCs of *Tlr5*$^{+/+}$ mice ($n = 5$) and *Tlr5*$^{-/-}$ mice ($n = 5$) on C57BL/6 background 48 h after oral infection with 5×10^8 *S. typhimurium*. CFU, colony-forming units. Data are one representative of three independent experiments (**a**,**b**) or are mean ± s.d. of triplicate samples from one representative of three independent experiments (**c**,**d**).

reported that DCs in the lamina propria are involved in oral tolerance induction[18,19]. Further study will help elucidate CD11c$^+$ LPC-mediated regulation of tolerance and host defense.

The second notable point was that TLR4 expression was very low in CD11c$^+$ LPCs. Most commensal bacteria in intestine are Gram-negative anaerobic rod bacteria, which contain LPS in their cell wall. It has been shown that CD11c$^+$ LPCs extend their dendrites to sample bacteria in the intestinal lumen[20]. Although the mechanism of bacterial sampling by CD11c$^+$ LPCs was fully analyzed, it has remained unclear how host intestinal mucosa remains tolerant to commensal bacteria and discriminates between commensal and pathogenic bacteria. Low expression of TLR4 may allow CD11c$^+$ LPCs to avoid inducing inappropriate immune responses after exposure to commensal bacteria. Instead, CD11c$^+$ LPCs induced inflammatory responses after exposure to pathogenic flagellated bacteria mainly via TLR5. Some commensal bacteria also have flagella, but CD11c$^+$ LPCs did not respond vigorously to those bacteria. In addition, it has been reported that some commensal bacteria, such as α- and ε-proteobacteria, change the TLR5-recognition site of flagellin without losing flagellar motility[21]. Furthermore, some commensal bacteria suppress flagellin expression in stable host environments[12]. Therefore, unlike pathogenic bacteria, commensal bacteria may have mechanisms to escape TLR5-mediated host detection.

Other TLR family members, such as TLR2 and TLR4, also recognize bacterial components. The importance of TLR2 and TLR4 in host defense against various bacteria has been demonstrated with *Tlr2*$^{-/-}$ mice and *Tlr4*$^{-/-}$ mice. In particular, C3H/HeJ mice, which express a mutant form of TLR4, are highly susceptible to intraperitoneal infection by *S. typhimurium*[1]. Because TLR5 is highly expressed exclusively in the intestine, we predicted that no there would be no substantial difference in the survival of *Tlr5*$^{+/+}$ and *Tlr5*$^{-/-}$ mice after intraperitoneal infection. Instead, we predicted that disruption of *Tlr5* would render mice more susceptible to oral *S. typhimurium* infection, because stimulation of TLR5 induced the production of proinflammatory cytokines in CD11c$^+$ LPCs. The resistance of *Tlr5*$^{-/-}$ mice to oral *S. typhimurium* infection was unexpected. *Tlr5*$^{-/-}$ mice survived longer than *Tlr5*$^{+/+}$ mice because of impaired transport of *S. typhimurium* from the intestinal tract to the liver and spleen. We believe that this unexpected result is closely related to specific pathogenesis of salomonella. Most reports have indicated that *S. typhimurium* are captured by subepithelial DCs after transport through M cells in Peyer's patches[22] or by intraepithelial DCs that send protrusions into the lumen of the small intestine[23]. After being internalized, *S. typhimurium* actively modulates host vesicular trafficking pathways to avoid delivery to lysosomes and to establish a specialized replicative niche[24]. Bacteria-laden DCs undergo maturation and migrate to T cell zones of Peyer's patches or draining MLNs[12]. These mature DCs are also thought to be responsible for the dissemination of *S. typhimurium* through the bloodstream to the liver and spleen[12,25]. The uptake of *S. typhimurium* in Peyer's patches and LPCs was the same in *Tlr5*$^{+/+}$ and *Tlr5*$^{-/-}$ mice. Furthermore, the uptake of *S. typhimurium* was the same in *Tlr5*$^{+/+}$ and *Tlr5*$^{-/-}$ CD11c$^+$ LPCs *in vitro* (data not shown). However, there were many fewer bacteria in MLNs of *Tlr5*$^{-/-}$ mice than in *Tlr5*$^{+/+}$ mice, suggesting that the transport of *S. typhimurium* from lamina propria to MLNs was impaired. As *S. typhimurium* could not fully activate and mature *Tlr5*$^{-/-}$ CD11c$^+$ LPCs, migration of *S. typhimurium*–laden CD11c$^+$ LPCs from the periphery to circulation may be inefficient in *Tlr5*$^{-/-}$ mice. In support of that idea, there were many fewer *S. typhimurium*–laden CD11c$^+$ cells in *Tlr5*$^{-/-}$ mice than in *Tlr5*$^{+/+}$ mice after infection. Although TLR5 on CD11c$^+$ LPCs initially sense flagellated pathogenic bacteria to induce host defense, facultative intracellular pathogens such as *S. typhimurium* may use CD11c$^+$ LPCs as carriers for systemic infection. Further study will be needed to clarify the mechanism of systemic *S. typhimurium* infection, through the generation of a specific marker for CD11c$^+$ LPCs or a technique to specifically effect depletion of these cells. Finally, our work is likely to open new therapeutic perspectives. New methods that target TLR5 on CD11c$^+$ LPCs would be useful for mucosal adjuvant immune therapies.

METHODS

Mice, reagents and bacteria. C57BL/6 mice were purchased from CLEA Japan. *Tlr4*$^{-/-}$ mice have been described[26]. *Tlr5*$^{-/-}$ mice are described in the **Supplementary Methods** online. All animal experiments were done with an experimental protocol approved by the Ethics Review Committee for Animal Experimentation of Research Institute for Microbial Diseases at Osaka University (Osaka, Japan). LPS from *Salmonella minnesota* Re595 was prepared with a phenol–chloroform–petroleum ether extraction procedure and purified flagellin was a gift from A. Aderem (Institute for Systems Biology, Seattle, Washington). *Salmonella enteritica* serovar typhimurium SR-11 x3181 and x3181 *fliA*::Tn*10* bacteria were provided by the Kitasato Institute for Life Science (Kitasato, Japan)[15,27]. *E. cloacae* was isolated from a healthy human volunteer and was identified by The Research Foundation for Microbial Diseases of Osaka University.

Cells. The preparation of GM-DCs and peritoneal macrophages has been described[28]. For the preparation of splenic macrophages and DCs, spleens were cut into small fragments and were incubated for 20 min at 37 °C with RPMI 1640 medium containing 400 U/ml of collagenase (Wako) and 15 μg/ml of DNase (Sigma). For the last 5 min, 5 mM EDTA was added. Single-cell suspensions were prepared after red blood cell lysis, and macrophages and DCs were positively selected with microbeads coated with antibody to CD11b (anti-CD11b) and anti-CD11 (Miltenyi), respectively. Intestinal lymphocytes and epithelial cells were isolated by a published protocol[9]. CD11c$^+$ cells from small intestine lamina propria and Peyer's patches were isolated by a published protocol[9].

Measurement of proinflammatory cytokines. GM-DCs, peritoneal macrophages, CD11b$^+$ splenocytes, CD11c$^+$ splenocytes and CD11c$^+$ LPCs were cultured in 96-well plates (5×10^4 cells/well) with LPS (100 ng/ml) or flagellin (1 μg/ml). The concentrations of tumor necrosis factor, IL-6, IL-12p40 and IL-10 in culture supernatants were measured by the Bio-Plex system (Bio-Rad) following the manufacturer's instructions.

PCR. RNA (1 μg) was reverse-transcribed with Superscript2 (Invitrogen) according to the manufacturer's instructions with random hexamers as primers. PCR used the primer pairs in **Supplementary Table 1** online and Taq polymerase (Takara Shuzo). After being incubated at 95 °C for 10 min, products were amplified by 25 cycles of 97 °C (30 s), 57 °C (30 s) and 72 °C (30 s). Products were analyzed by agarose gel electrophoresis. Quantitative real-time PCR was done with a final volume of 25 μl containing cDNA amplified as described above, 2x PCR Master Mix (Applied Biosystems) and primers for 18S rRNA (Applied Biosystems) as an internal control or primers specific for *Tlr4* or *Tlr5* (Assay on Demand), using a 7700 Sequence Detector (Applied Biosystems). After being incubated at 95 °C for 10 min, products were amplified by 35 cycles of 95 °C (15 s), 60 °C (60 s) and 50 °C (120 s).

Microarray analysis. IECs and LPCs collected from *Tlr5*$^{+/+}$ and *Tlr5*$^{-/-}$ mice were left untreated or were treated for 4 h with flagellin (1 μg/ml). Total RNA was extracted with an RNeasy kit (Qiagen) and was purified with an Oligotex mRNA Kit (Pharmacia). Fragmented and biotin-labeled cDNA was synthesized from 100 ng purified mRNA with the Ovation Biotin System (Nugen) according to the manufacturer's protocol. The cDNA was hybridized to Affymetrix Murine Genome 430 2.0 microarray chips (Affymetrix) according to the manufacturer's instructions. Hybridized chips were stained and washed and were scanned with a GeneArray Scanner (Affymetrix). Microarray Suite software (Version 5.0, Affymetrix) and GeneSpring software (Silicon Genetics) were used for data analysis.

Immunofluorescence. Biotinylated monoclonal anti–mouse CD11c (HL3; Pharmingen) and anti-TLR5 (AP1505a; Abgent) were applied overnight at 4 °C to sections cut from frozen intestinal tissue. Samples were washed and then were incubated for 2 h at 25 °C with streptavidin–Alexa Fluor 594 (S-32356; Molecular Probes) and Alexa Fluor 488–chicken anti–rabbit IgG (A-21441; Molecular Probes). Staining was analyzed with a Radiance2100 laser-scanning confocal microscope (Bio-Rad). The intestinal loop assay is described in the **Supplementary Methods**.

Bacterial infection. *S. typhimurium* was grown in Luria-Bertani medium without shaking at 37 °C. The concentration of bacteria was determined by the absorbance at 600 nm. Bacteria were injected orally or intraperitoneally into 8-week-old mice. For determination of the bacterial burden in livers and spleens, LPCs, PPCs and MLNs were lysed with 0.01% Triton-X100. Serial dilutions of lysates were plated on Luria-Bertani agar plates and colonies were counted after overnight incubation at 37 °C.

Statistics. Kaplan-Meier plots and log-rank tests were used to assess the survival differences of control and mutant mice after bacterial infection.

Accession code. GEO: microarray data, GSE5119.

Note: Supplementary information is available on the Nature Immunology website.

ACKNOWLEDGMENTS

We thank K. Smith and T. Hawn (Institute for Systems Biology, Seattle, Washington) for providing purified flagellin; C. Sasagawa and T. Suzuki (Institute of Medical Science, Tokyo, Japan) for providing bacteria; members of the DNA-chip Development Center for Infectious Diseases (RIMD, Osaka University, Osaka, Japan) for technical advice; N. Kitagaki for technical assistance; and M. Hashimoto for secretarial assistance. Supported by Special Coordination Funds, the Ministry of Education, Culture, Sports, Science and Technology, and Research Fellowships of the Japan Society for the Promotion of Science for Young Scientists.

AUTHOR CONTRIBUTIONS

S.U. and M.H.J. did most of the experiments to characterize mouse phenotypes; N.C. helped with the quantitative PCR, microarray analysis, isolation of cells and enzyme-linked immunosorbent assays; Z.G. helped to isolate cells and with immunostaining and did the surgical operations for the intestinal loop assay; Y.K. helped with analysis of microarray data; M.Y. helped to generate *Tlr5*$^{-/-}$ mice; H.K. helped with the enzyme-linked immunosorbent assays; N.S. helped to isolate cells; H.M. provided *S. typhimurium* and provided instructions for infection experiments; H.K. helped with the infection experiments; H.H. helped to generate *Tlr5*$^{-/-}$ mice; C.C. helped with the infection experiments; T.K., K.J.I. and O.T. provided advice for the experiments; M.M. provided advice for the experiments and manuscript; K.T. helped to generate *Tlr5*$^{-/-}$ mice and to design experiments; and S.A. designed all the experiments and prepared the manuscript.

COMPETING INTERESTS STATEMENT

The authors declare that they have no competing financial interests.

Published online at http://www.nature.com/natureimmunology/
Reprints and permissions information is available online at http://npg.nature.com/reprintsandpermissions/

1. Akira, S., Uematsu, S. & Takeuchi, O. Pathogen recognition and innate immunity. *Cell* **124**, 783–801 (2006).
2. Hayashi, F. *et al.* The innate immune response to bacterial flagellin is mediated by Toll-like receptor 5. *Nature* **410**, 1099–1103 (2001).
3. Macnab, R.M. Genetics and biogenesis of bacterial flagella. *Annu. Rev. Genet.* **26**, 131–158 (1992).
4. Gewirtz, A.T., Navas, T.A., Lyons, S., Godowski, P.J. & Madara, J.L. Cutting edge: bacterial flagellin activates basolaterally expressed TLR5 to induce epithelial proinflammatory gene expression. *J. Immunol.* **167**, 1882–1885 (2001).
5. Salazar-Gonzalez, R.M. & McSorley, S.J. Salmonella flagellin, a microbial target of the innate and adaptive immune system. *Immunol. Lett.* **101**, 117–122 (2005).
6. Sierro, F. *et al.* Flagellin stimulation of intestinal epithelial cells triggers CCL20-mediated migration of dendritic cells. *Proc. Natl. Acad. Sci. USA* **98**, 13722–13727 (2001).
7. Sebastiani, G. *et al.* Cloning and characterization of the murine toll-like receptor 5 (*Tlr5*) gene: sequence and mRNA expression studies in Salmonella-susceptible MOLF/Ei mice. *Genomics* **64**, 230–240 (2000).
8. Hawn, T.R. *et al.* A common dominant TLR5 stop codon polymorphism abolishes flagellin signaling and is associated with susceptibility to legionnaires' disease. *J. Exp. Med.* **198**, 1563–1572 (2003).
9. Jang, M.H. *et al.* CCR7 is critically important for migration of dendritic cells in intestinal lamina propria to mesenteric lymph nodes. *J. Immunol.* **176**, 803–810 (2006).
10. Gewirtz, A.T. *et al.* Salmonella typhimurium translocates flagellin across intestinal epithelia, inducing a proinflammatory response. *J. Clin. Invest.* **107**, 99–109 (2001).
11. Pavli, P., Woodhams, C.E., Doe, W.F. & Hume, D.A. Isolation and characterization of antigen-presenting dendritic cells from the mouse intestinal lamina propria. *Immunology* **70**, 40–47 (1990).
12. Niedergang, F., Didierlaurent, A., Kraehenbuhl, J.P. & Sirard, J.C. Dendritic cells: the host Achille's heel for mucosal pathogens? *Trends Microbiol.* **12**, 79–88 (2004).
13. Ruedl, C., Rieser, C., Bock, G., Wick, G. & Wolf, H. Phenotypic and functional characterization of CD11c^{+} dendritic cell population in mouse Peyer's patches. *Eur. J. Immunol.* **26**, 1801–1806 (1996).
14. Wakkach, A. *et al.* Characterization of dendritic cells that induce tolerance and T regulatory 1 cell differentiation in vivo. *Immunity* **18**, 605–617 (2003).
15. Kutsukake, K., Ohya, Y., Yamaguchi, S. & Iino, T. Operon structure of flagellar genes in Salmonella typhimurium. *Mol. Gen. Genet.* **214**, 11–15 (1988).
16. Mayrhofer, G., Pugh, C.W. & Barclay, A.N. The distribution, ontogeny and origin in the rat of Ia-positive cells with dendritic morphology and of Ia antigen in epithelia, with special reference to the intestine. *Eur. J. Immunol.* **13**, 112–122 (1983).
17. Mowat, A.M. Anatomical basis of tolerance and immunity to intestinal antigens. *Nat. Rev. Immunol.* **3**, 331–341 (2003).
18. Chirdo, F.G., Millington, O.R., Beacock-Sharp, H. & Mowat, A.M. Immunomodulatory dendritic cells in intestinal lamina propria. *Eur. J. Immunol.* **35**, 1831–1840 (2005).
19. Worbs, T. *et al.* Oral tolerance originates in the intestinal immune system and relies on antigen carriage by dendritic cells. *J. Exp. Med.* **203**, 519–527 (2006).
20. Niess, J.H. *et al.* CX3CR1-mediated dendritic cell access to the intestinal lumen and bacterial clearance. *Science* **307**, 254–258 (2005).
21. Andersen-Nissen, E. *et al.* Evasion of Toll-like receptor 5 by flagellated bacteria. *Proc. Natl. Acad. Sci. USA* **102**, 9247–9252 (2005).
22. Hopkins, S.A., Niedergang, F., Corthesy-Theulaz, I.E. & Kraehenbuhl, J.P. A recombinant Salmonella typhimurium vaccine strain is taken up and survives within murine Peyer's patch dendritic cells. *Cell. Microbiol.* **2**, 59–68 (2000).
23. Rescigno, M. *et al.* Dendritic cells express tight junction proteins and penetrate gut epithelial monolayers to sample bacteria. *Nat. Immunol.* **2**, 361–367 (2001).
24. Patel, J.C., Rossanese, O.W. & Galan, J.E. The functional interface between Salmonella and its host cell: opportunities for therapeutic intervention. *Trends Pharmacol. Sci.* **26**, 564–570 (2005).
25. Vazquez-Torres, A. *et al.* Extraintestinal dissemination of Salmonella by CD18-expressing phagocytes. *Nature* **401**, 804–808 (1999).
26. Hoshino, K. *et al.* Cutting edge: Toll-like receptor 4 (TLR4)-deficient mice are hyporesponsive to lipopolysaccharide: evidence for TLR4 as the Lps gene product. *J. Immunol.* **162**, 3749–3752 (1999).
27. Gulig, P.A. & Curtiss, R., III Plasmid-associated virulence of *Salmonella typhimurium*. *Infect. Immun.* **55**, 2891–2901 (1987).
28. Hemmi, H., Kaisho, T., Takeda, K. & Akira, S. The roles of Toll-like receptor 9, MyD88, and DNA-dependent protein kinase catalytic subunit in the effects of two distinct CpG DNAs on dendritic cell subsets. *J. Immunol.* **170**, 3059–3064 (2003).

nature immunology

Key function for the Ubc13 E2 ubiquitin-conjugating enzyme in immune receptor signaling

Masahiro Yamamoto[1], Toru Okamoto[2], Kiyoshi Takeda[3], Shintaro Sato[4], Hideki Sanjo[1], Satoshi Uematsu[1], Tatsuya Saitoh[1,5], Naoki Yamamoto[5], Hiroaki Sakurai[6], Ken J Ishii[4], Shoji Yamaoka[5], Taro Kawai[4], Yoshiharu Matsuura[2], Osamu Takeuchi[1,4] & Shizuo Akira[1,4]

The Ubc13 E2 ubiquitin-conjugating enzyme is key in the process of 'tagging' target proteins with lysine 63–linked polyubiquitin chains, which are essential for the transmission of immune receptor signals culminating in activation of the transcription factor NF-κB. Here we demonstrate that conditional ablation of Ubc13 resulted in defective B cell development and in impaired B cell and macrophage activation. In response to all tested stimuli except tumor necrosis factor, Ubc13-deficient cells showed almost normal NF-κB activation but considerably impaired activation of mitogen-activated protein kinase. Ubc13-induced activation of mitogen-activated protein kinase required, at least in part, ubiquitination of the adaptor protein IKKγ. These results show that Ubc13 is key in the mammalian immune response.

Stimulation of Toll-like receptors (TLRs), interleukin 1 receptor (IL-1R), antigen receptors, CD40 and tumor necrosis factor receptor (TNFR) results in activation of mitogen-activated protein (MAP) kinases and of the transcription factor NF-κB. Such signals induce immune cell proliferation and survival and cytokine production[1]. In unstimulated cells, IκB proteins sequester NF-κB in the cytoplasm. Immune stimuli result in phosphorylation and ubiquitin- and proteasome-dependent degradation of IκB, thereby permitting translocation of NF-κB to the nucleus[2]. MAP kinases such as c-Jun N-terminal kinase (Jnk) and p38 are rapidly phosphorylated and activated by corresponding 'upstream' MAP kinase kinases, which are activated by MAP kinase kinase kinases. More than ten MAP kinase kinase kinases have been identified[3].

TLRs and IL-1R share 'downstream' signaling molecules, including MyD88, IL-1R-associated kinases (IRAKs) and TNFR-associated factor 6 (TRAF6)[4]. Genetic and biochemical studies suggest that TRAF6, the most distal of these shared signaling proteins, is pivotal in the TLR, IL-1R and CD40 signaling pathways[5]. Moreover, another TRAF family member, TRAF2, is required for TNFR signaling. These observations indicate the convergent function of the TRAF family members in innate immune signaling pathways[6]. Stimulation of B cell receptors (BCRs) and T cell receptors (TCRs) also activates NF-κB and MAP kinases[7]. Adaptor proteins such as Bcl-10, CARMA1 (also called CARD11 or Bimp3) and MALT1 (also called paracaspase) are required for BCR- and TCR-induced NF-κB and MAP kinase activation[8–14]. *In vitro* studies suggest that TRAF2 and TRAF6 are also involved in antigen receptor signaling[15].

TRAF2 and TRAF6 contain N-terminal RING finger domains that have E3 ubiquitin ligase activity[16]. Stimulus-dependent ubiquitination of TRAF6 activates the MAP kinase kinase kinase TGF-β-activated kinase (TAK1), which is critical in the activation of NF-κB and MAP kinases[17–19]. Moreover, TRAF6- and TRAF2-dependent ubiquitination of the adaptor protein IKKγ (also called NEMO) is involved in antigen receptor–induced NF-κB activation[15]. Polyubiquitin chains appended to TRAF and IKKγ are formed through linkages at lysine 63 (K63) of ubiquitin[20].

In contrast to lysine 48 (K48)–linked polyubiquitin chains, which induce proteasome-dependent degradation of the target proteins to which they are appended, K63-linked polyubiquitin chains have been linked to biological processes such as the stress response and DNA repair, rather than protein destruction[21]. K63-linked polyubiquitin chains are reportedly generated by the E2 ubiquitin-conjugating enzyme Ubc13 (ref. 22). The gene encoding Ubc13 was originally identified as being responsible for defective neural development in a drosophila mutant called *bendless*[23]. Subsequently, the synthesis of TRAF2- and TRAF6-dependent K63-linked polyubiquitin chains has been shown to be catalyzed by Ubc13 and Uev1A[16]. RNA silencing of the gene encoding Ubc13 results in defective NF-κB activation in HEK293 cells and insect cells[15,24–27], suggesting that the main function of Ubc13 is in NF-κB activation. In contrast, expression of dominant negative Ubc13 marginally affects TNF-induced NF-κB activation[28],

[1]Department of Host Defense and [2]Department of Molecular Virology, Research Institute for Microbial Diseases, Osaka University, Osaka 565-0871, Japan. [3]Department of Embryonic and Genetic Engineering, Medical Institute of Bioregulation, Kyushu University, Fukuoka 812-8582, Japan. [4]ERATO, Japan Science and Technology Corporation, Osaka 565-0871, Japan. [5]Department of Molecular Virology, Graduate School of Medicine, Tokyo Medical and Dental University, Tokyo 113-8519, Japan. [6]Division of Pathogenic Biochemistry, Institute of Natural Medicine, 21st Century Center of Excellence Program, Toyama Medical and Pharmaceutical University, Toyama 930-0194, Japan. Correspondence should be addressed to Shizuo Akira (sakira@biken.osaka-u.ac.jp).

Received 21 February; accepted 29 June; published online 23 July 2006; doi:10.1038/ni1367

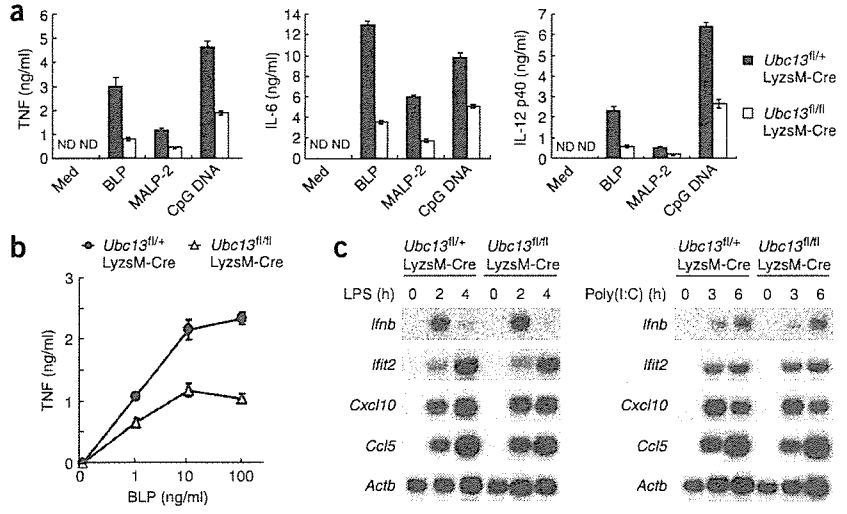

Figure 1 Defective proinflammatory cytokine production in Ubc13-deficient bone marrow macrophages. (**a**) ELISA of IL-6, TNF and IL-12p40 in culture supernatants of bone marrow macrophages (mouse genotypes, key) cultured for 24 h with 100 ng/ml of BLP, 30 ng/ml of MALP-2 or 1 μM CpG DNA in the presence of 30 ng/ml of interferon-γ. Med, medium only; ND, not detected. (**b**) ELISA of TNF in culture supernatants of bone marrow macrophages (mouse genotypes, key) cultured for 24 h with BLP (concentration, horizontal axis) in the presence of 30 ng/ml of interferon-γ. Data (**a**,**b**) represent mean ± s.d. of triplicate samples and are representative of three independent experiments. (**c**) RNA blot analysis of total RNA (10 μg) extracted from bone marrow macrophages (mouse genotypes, above blots) stimulated with 100 ng/ml of LPS (left) or 50 μg/ml of poly(I:C) (right). *Ifnb*, *Ifit2*, *Cxcl10*, *Ccl5* and *Actb* encode interferon-β, ISG54, IP-10, RANTES and β-actin, respectively. Data are representative of two independent experiments.

and the RING finger domain of TRAF6, which is essential for ligation of K63-linked polyubiquitin chains to target proteins, is dispensable for the IL-1R- and TLR-mediated NF-κB activation[29]. Those results suggest that Ubc13 has a minor function in NF-κB activation. Thus, whether Ubc13 is essential for immune signaling and immune responses *in vivo* is not known.

Here we have generated mice conditionally deficient in Ubc13. We demonstrate that Ubc13 was essential for TLR-induced proinflammatory cytokine production in bone marrow–derived macrophages. In addition, Ubc13 was required for TLR-, CD40- and BCR-induced B cell activation. B cell–specific deletion of Ubc13 resulted in defective development of marginal zone B cells and B-1 cells and in impaired humoral immune responses. Ubc13-deficient cells had almost normal NF-κB activation and normal TAK1 phosphorylation. In contrast, Ubc13-deficient cells had substantially impaired MAP kinase activation in response to all stimuli tested, except for TNF. Ubc13-induced MAP kinase activation was mediated partially through ubiquitination of IKKγ, which was abolished in Ubc13-deficient cells. Our results demonstrate the physiological importance of Ubc13 in the induction of mammalian immune responses.

RESULTS

Conditional ablation of Ubc13

To assess the function of Ubc13 in adult mice, we generated mice in which Ubc13 could be conditionally ablated (**Supplementary Fig. 1** online). The gene encoding Ubc13 (called '*Ubc13*' here) consists of four exons. We constructed a targeting vector to insert *lox*P sites flanking exons 2, 3 and 4 of *Ubc13* and to insert a *lox*P-flanked neomycin-resistance gene into intron 1 of *Ubc13*. To generate conventional Ubc13-deficient ($Ubc13^{-/-}$) mice, we constructed another targeting vector lacking the flanked exons (data not shown). In both cases, we microinjected two correctly targeted embryonic stem cell clones into C57BL/6 blastocysts to generate chimeric mice. We crossed male chimeric with female C57BL/6 mice and monitored transmission of the mutated allele by Southern blot analysis (**Supplementary Fig. 1** and data not shown). Although $Ubc13^{+/-}$ mice were phenotypically normal and fertile, we failed to obtain $Ubc13^{-/-}$ offspring by intercrossing $Ubc13^{+/-}$ mice (**Supplementary Table 1** online). To determine the time of death *in utero*, we genotyped embryos from $Ubc13^{+/-}$ intercrosses at embryonic day 13.5 or 9.5. We detected no $Ubc13^{-/-}$ embryos, indicating that Ubc13 deficiency results in early embryonic death. In contrast, mice homozygous for *lox*P-flanked *Ubc13* alleles ($Ubc13^{fl/fl}$ mice) were born at the expected mendelian ratios and had no obvious abnormalities (data not shown).

Ubc13 in macrophage activation

Because Ubc13 has been linked to the activation of TRAF6, a crucial component of TLR signaling pathways[16,30], we assessed the function of Ubc13 in the TLR responses in bone marrow–derived macrophages. To disrupt *Ubc13* specifically in macrophages, were crossed $Ubc13^{fl/fl}$ mice with mice in which cDNA encoding Cre recombinase is inserted into the gene encoding lysozyme M, which is specifically expressed in the myeloid linage such as macrophages and granulocytes (LyzsM-Cre mice). Southern blot analysis showed that in bone marrow macrophages from the resultant '$Ubc13^{fl/fl}$LyzsM-Cre mice', Cre-mediated deletion produced a new 1.1-kb band corresponding to the mutated *Ubc13* allele, and immunoblot analysis showed that $Ubc13^{fl/fl}$LyzsM-Cre bone marrow macrophages had much less Ubc13 protein than did control cells (**Supplementary Fig. 1**).

Bone marrow macrophages produce proinflammatory cytokines in response to a variety of TLR ligands in a MyD88-dependent way[4]. Thus, we assessed cytokine production by $Ubc13^{fl/fl}$LyzsM-Cre bone marrow macrophages stimulated with TLR ligands such as BLP, MALP-2 and CpG DNA. Bone marrow macrophages from $Ubc13^{fl/fl}$LyzsM-Cre mice produced less TNF, IL-6 and IL-12p40 than did those from control mice (**Fig. 1a**), and the response to BLP was dose dependent (**Fig. 1b**). These results indicate that Ubc13 is important in TLR-induced cytokine production in bone marrow macrophages.

TLR signaling can be MyD88 dependent or MyD88 independent. MyD88-independent TLR3 and TLR4 signaling results in the induction of type I interferon and interferon-inducible genes[4]. To assess the function of Ubc13 in MyD88-independent immune responses, we analyzed expression of the gene encoding interferon-β and of interferon-inducible genes, including *Ifit2*, *Cxcl10* and *Ccl5*, after treatment of control or $Ubc13^{fl/fl}$LyzsM-Cre bone marrow macrophages with lipopolysaccharide (LPS) or poly(I:C). Control and $Ubc13^{fl/fl}$LyzsM-Cre bone marrow macrophages contained similar amounts of transcripts encoding interferon and of interferon-inducible gene transcripts after LPS or poly(I:C) stimulation, indicating that

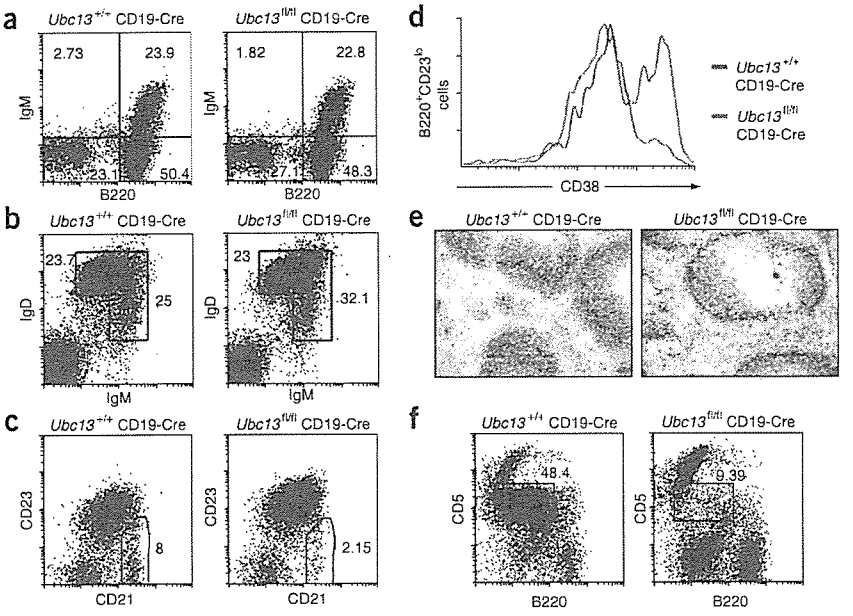

Figure 2 Impaired B cell development in *Ubc13*$^{fl/fl}$Cd19-Cre mice. (**a–d**) Flow cytometry of IgM and B220 expression by B cell precursors in the bone marrow (**a**) and of IgM and IgD expression (**b**), CD21 and CD23 expression by B220$^+$ populations (**c**) and CD38 expression by B220$^+$CD23^{lo} populations (**d**) of B cells in the spleens of 6- to 10-week-old mice. (**e**) Frozen splenic sections stained with rat monoclonal antibody to mouse metallophilic macrophages (red) and with anti-B220 to visualize B cells (blue). Original magnification, ×200. (**f**) Flow cytometry of B220 and CD5 expression by CD5$^+$ B cells in the peritonea of 6- to 10-week-old mice. Numbers in dot plots indicate percentages of cells in each quadrant (**a**); of mature (**b**, left) and immature (**b**, right) splenic B cells; of marginal zone B cells (**c**); and of B1 cells (**f**). Data are representative of three independent experiments.

Ubc13 is dispensable for the TLR-mediated MyD88-independent immune responses in bone marrow macrophages (**Fig. 1c**).

Ubc13 in B cell development and function

Mice lacking molecules involved in BCR signaling show defective B cell development. Specifically, mice lacking the Bcl-10 or MALT1 adaptor proteins show defective development of marginal zone B cells and B-1 B cells[9,13,31]. The adaptor protein CARMA1 is also essential for the generation of B-1 B cells[10–12,14]. To determine whether Ubc13 deficiency affects the B cell development, we generated mice lacking Ubc13 specifically in the B cell lineage. We crossed *Ubc13*$^{fl/fl}$ mice with mice expressing a Cre transgene under control of the *Cd19* promoter (Cd19-Cre mice). Southern blot and immunoblot analysis showed almost complete Cre-mediated deletion of the *Ubc13* *lox*P-flanked alleles and the protein in splenic B220$^+$ cells from these '*Ubc13*$^{fl/fl}$ Cd19-Cre mice' (**Supplementary Fig. 1**).

To determine whether the Ubc13 disruption affected B cell development, we examined the bone marrow of control and *Ubc13*$^{fl/fl}$Cd19-Cre mice. Control and *Ubc13*$^{fl/fl}$Cd19-Cre mice had no differences in bone marrow cellularity, and B cell precursor populations in control and *Ubc13*$^{fl/fl}$Cd19-Cre mice had similar expression of surface B220 and immunoglobulin M (IgM; **Fig. 2a**). Moreover, splenocytes from *Ubc13*$^{fl/fl}$Cd19-Cre mice had a pattern of surface expression of CD3 and B220 similar to that of control mice (**Supplementary Fig. 2** online). Whereas the expression of IgM and IgD was similar on the surfaces of splenocytes from control and *Ubc13*$^{fl/fl}$Cd19-Cre mice (**Fig. 2b**), *Ubc13*$^{fl/fl}$Cd19-Cre mice had a much lower frequency of B220$^+$CD21^{hi}CD23^{lo} marginal zone B cells (**Fig. 2c**). Detection of marginal zone B cells with another set of surface antigens, B220, CD38 and CD21, produced similar results (**Fig. 2d**). Immunohistochemical staining confirmed that the width of marginal zone B cell area was smaller in spleens from *Ubc13*$^{fl/fl}$Cd19-Cre mice (**Fig. 2e**). The CD5$^+$ peritoneal B-1 cell population was also much lower in *Ubc13*$^{fl/fl}$Cd19-Cre mice (**Fig. 2f**). These results suggest that Ubc13 is essential for the development of marginal zone B cells and peritoneal CD5$^+$ B-1 cells.

To test whether Ubc13 is involved in TLR responses in B cells, we analyzed the proliferation of control and *Ubc13*$^{fl/fl}$Cd19-Cre B cells stimulated with LPS or CpG DNA. Control B cells proliferated in a dose-dependent way in response to both LPS and CpG DNA stimulation (**Fig. 3a**). In contrast, proliferation of *Ubc13*$^{fl/fl}$Cd19-Cre B cells in response to these stimuli was much lower. In addition, CpG DNA–induced IL-6 production in *Ubc13*$^{fl/fl}$Cd19-Cre B cells was severely impaired (**Fig. 3b**). Compared with control B cells, *Ubc13*$^{fl/fl}$Cd19-Cre B cells also showed defective proliferation in response to stimulation with antibody to IgM (anti-IgM) or anti-CD40 (**Fig. 3a**). We next assessed whether these defects in TLR-, BCR- and CD40-mediated proliferation were accompanied by impaired cell cycle progression in *Ubc13*$^{fl/fl}$Cd19-Cre B cells. Compared with control B cells, which entered S phase after stimulation with LPS, CpG DNA, anti-IgM or anti-CD40, fewer *Ubc13*$^{fl/fl}$Cd19-Cre B cells entered S phase after stimulation (**Fig. 3c**). Stimulation with LPS, CpG DNA or anti-CD40 can prevent B cell apoptosis that normally results from *ex vivo* culture of B cells without mitogens[19]. A greater proportion of *Ubc13*$^{fl/fl}$Cd19-Cre B cells than control B cells underwent apoptosis *ex vivo*, even after stimulation with LPS, CpG DNA or anti-CD40 (**Fig. 3d**). These results collectively suggest that Ubc13 is critical for TLR-, BCR-, and CD40-mediated B cell activation, proliferation and survival.

To investigate whether the defective activation and development of *Ubc13*$^{fl/fl}$Cd19-Cre B cells affected on the immune responses *in vivo*, we compared immunoglobulin concentrations in sera of control and *Ubc13*$^{fl/fl}$Cd19-Cre mice (**Fig. 3e**). All immunoglobulin isotypes tested except IgG2a and IgG2b were significantly lower in *Ubc13*$^{fl/fl}$ Cd19-Cre mice than in control mice. After immunization with the T cell–independent polyvalent antigen trinitrophenol-Ficoll or the T cell–dependent antigen nitrophenol–chicken γ-globulin, *Ubc13*$^{fl/fl}$ Cd19-Cre mice had significantly less serum trinitrophenol-specific IgM and IgG3 (**Fig. 3f**). Although nitrophenol-specific IgM titers were similar, nitrophenol-specific IgG1 titers were lower in *Ubc13*$^{fl/fl}$Cd19-Cre mice (**Fig. 3g**). Thus, Ubc13 is required for appropriate humoral immune responses *in vivo*.

Ubc13 in NF-κB and MAPK activation

TLR, BCR, CD40, IL-1R and TNFR signals culminate in NF-κB activation[32]. Although *in vitro* studies indicate that Ubc13 is involved in NF-κB activation in HEK293 cells[33], whether Ubc13 deficiency affects NF-κB activation mediated by TLR, BCR, CD40, TNFR or IL-1R in other cell types in physiological conditions is not known.

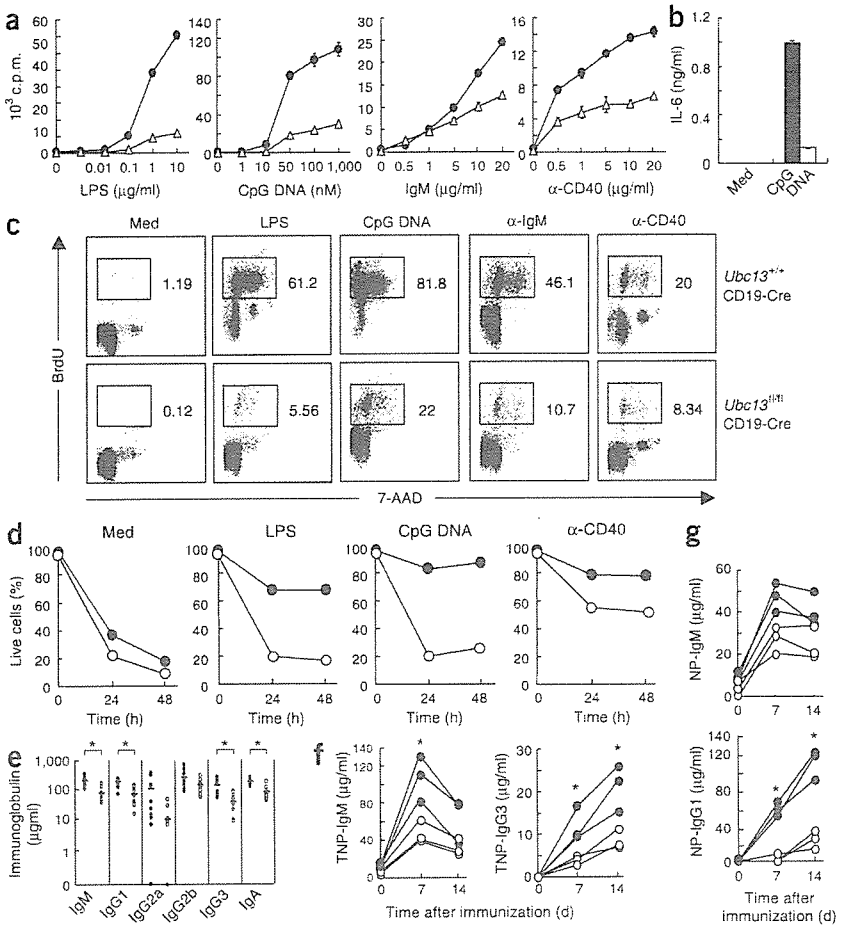

Figure 3 Ubc13 is required for B cell activation and *in vivo* immune responses. (**a**) Proliferation of splenic B220$^+$ B cells cultured for 48 h with various stimuli (horizontal axes). α-CD40, anti-CD40. Data are representative of three independent experiments. (**b**) ELISA of IL-6 in supernatants of splenic B220$^+$ B cells stimulated for 48 h with 1 μM CpG DNA. ND, not detected. Data represent mean ± s.d. of triplicate samples and are representative of two independent experiments. (**c**) Cell cycle profiles of B cells stimulated with 10 μg/ml of LPS, 1 μM CpG DNA, 10 μg/ml of anti-IgM or 10 μg/ml of anti-CD40. Cells labeled with 5-bromodeoxyuridine (BrdU) and 7-amino-actinomycin D (7-AAD) were analyzed by flow cytometry 24 h after stimulation. Numbers beside boxed areas indicate percentages of cells in S phase. Data are representative of two independent experiments. (**d**) Viability of B cells stimulated with 10 μg/ml of LPS, 1 μM CpG DNA or 10 μg/ml of anti-CD40, as assessed by annexin V staining (time, horizontal axes). Data are representative of three independent experiments. (**e**) ELISA of immunoglobulin isotypes in the sera of unimmunized 8-week-old mice ($n = 10$ mice of each genotype). Each symbol represents one mouse. *, $P < 0.05$ (Student's *t*-test). (**f**) Production of trinitrophenol-specific IgM (TNP-IgM) and IgG3 (TNP-IgG3) at 7 and 14 d after immunization with trinitrophenol-Ficoll. (**g**) Production of nitrophenol-specific IgM (NP-IgM) and IgG1 (NP-IgG1) at 7 and 14 d after immunization with nitrophenol–chicken γ-globulin. Results in **f**,**g** represent three of five mice per genotype; *, $P < 0.05$ (Student's *t*-test). Filled symbols or bars, *Ubc13*$^{+/+}$Cd19-Cre; open symbols or bars, *Ubc13*$^{fl/fl}$Cd19-Cre.

LPS, CpG DNA, anti-IgM and anti-CD40 resulted in slightly defective IκBα degradation but normal NF-κB nuclear translocation in *Ubc13*$^{fl/fl}$Cd19-Cre B cells (**Fig. 4a,b**). Nuclear NF-κB complexes contained similar NF-κB subunits in wild-type and *Ubc13*$^{fl/fl}$Cd19-Cre B cells (**Supplementary Fig. 3** online). In addition, BLP- and CpG DNA–mediated IκBα degradation NF-κB nuclear translocation was indistinguishable in control versus *Ubc13*$^{fl/fl}$LyzsM-Cre bone marrow macrophages (**Fig. 4c,d**). To determine whether Ubc13 is involved in TNFR- and IL-1R-mediated signal transduction, we generated mouse embryonic fibroblasts (MEFs) from control and *Ubc13*$^{fl/fl}$ embryos. Retroviral transduction of Cre into *Ubc13*$^{fl/fl}$ MEFs induced efficient deletion of Ubc13 protein (**Supplementary Fig. 1**). *Ubc13*$^{fl/fl}$ MEFs expressing retroviral Cre had normal TNF- and IL-1β-induced IκBα degradation and NF-κB nuclear translocation (**Fig. 4e,f**). To further investigate whether Ubc13 deficiency is dispensable for NF-κB activation, we transfected an NF-κB-dependent luciferase reporter construct into control or *Ubc13*$^{fl/fl}$ MEFs expressing retroviral Cre. TNF or IL-1β stimulation induced similar luciferase activity in control and *Ubc13*$^{fl/fl}$ MEFs (**Fig. 4g**). Moreover, overexpression of Bcl-10 or CARMA1 resulted in similar NF-κB activation in control and *Ubc13*$^{fl/fl}$ MEFs (**Fig. 4h**). In addition, IL-1β-induced IκBα recovery at later time points was similar for control and *Ubc13*$^{fl/fl}$ MEFs expressing retroviral Cre (**Fig. 4i**). To analyze the function of Ubc13 in alternative pathways of NF-κB activation, we assessed stimulus-dependent processing of the NF-κBp100 subunit. Control and *Ubc13*$^{fl/fl}$Cd19-Cre B cells had similar patterns of processing of NF-κBp100 to NF-κBp52 after stimulation with anti-CD40 or B cell–activating factor of the TNF family (**Supplementary Fig. 3**), indicating that Ubc13 is not involved in the alternative pathway of NF-κB activation. These data collectively suggest that although Ubc13 deficiency slightly affected IκBα degradation in some cell types, Ubc13 seems to be mostly dispensable for NF-κB activation.

Next we investigated activation of the Jnk, p38 and Erk MAP kinases in B cells, bone marrow macrophages and MEFs. Stimulation of control B cells with anti-IgM resulted in phoshorylation of Jnk, p38 and Erk. In contrast, although Erk activation was normal, anti-IgM-induced phoshorylation of Jnk and p38 was substantially impaired in *Ubc13*$^{fl/fl}$Cd19-Cre B cells. Moreover, *Ubc13*$^{fl/fl}$Cd19-Cre B cells had considerably reduced activation of all three MAP kinases in response to LPS and CpG DNA, and anti-CD40-induced MAP kinase activation was also mildly affected by Ubc13 deficiency (**Fig. 5a**). Although stimulation with BLP or CpG DNA resulted in rapid phosphorylation of MAP kinases in control bone marrow macrophages, MAP kinase activation in *Ubc13*$^{fl/fl}$LyzsM-Cre bone marrow macrophages was impaired (**Fig. 5b**). Furthermore, IL-1β-induced phosphorylation of Jnk, p38 and Erk was much lower in *Ubc13*$^{fl/fl}$ than in control MEFs expressing retroviral Cre (**Fig. 5c**). In contrast, TNF stimulation resulted in similar MAP kinase activation in *Ubc13*$^{fl/fl}$ and control MEFs expressing retroviral Cre (**Fig. 5d**). These results collectively demonstrate that Ubc13 is important in MAP kinase activation induced by TLR, IL-1R, BCR and CD40, but not MAP kinase activation induced by TNFR.